

Accepted for publication in AJ; to appear April 2001

The Mass and Structure of the Pleiades Star Cluster from 2MASS

Joseph D. Adams^{1,2}

University of Massachusetts, Department of Astronomy, LGRT 531-A, Amherst, MA 01003

John R. Stauffer³

Harvard-Smithsonian Center for Astrophysics, 60 Garden Street, Cambridge, MA 01238

David G. Monet

U.S. Naval Observatory Flagstaff Station, P.O. Box 1149, Flagstaff, AZ 86002-1149

`dgm@nofs.navy.mil`

Michael F. Skrutskie

University of Massachusetts, Department of Astronomy, LGRT 532, Amherst, MA 01003

`skrutski@astro.umass.edu`

and

Charles A. Beichman

Jet Propulsion Laboratory, California Institute of Technology, JPL 180-703, Pasadena, CA 91109

`chas@pop.jpl.nasa.gov`

ABSTRACT

We present the results of a large scale search for new members of the Pleiades star cluster using 2MASS near-infrared photometry and proper motions derived from POSS

¹Visiting Astronomer, Kitt Peak National Observatory, National Optical Astronomy Observatories, which is operated by the Association of Universities for Research in Astronomy, Inc. (AURA) under cooperative agreement with the National Science Foundation.

²Present address: Boston University, Institute for Astrophysical Research, 725 Commonwealth Avenue, Boston, MA 02215; e-mail: `jdadams@bu.edu`

³Present address: Infrared Processing and Analysis Center, California Institute of Technology, Mail Code 100-22, Pasadena, CA 91125; e-mail: `stauffer@ipac.caltech.edu`

plates digitized by the USNO PMM program. The search extends to a 10° radius around the cluster, well beyond the presumed tidal radius, to a limiting magnitude of $R \sim 20$, corresponding to $\sim 0.07 M_\odot$ at the distance and age of the Pleiades. Multi-object spectroscopy for 528 candidates verifies that the search was extremely effective at detecting cluster stars in the 1 - $0.1 M_\odot$ mass range using the distribution of H α emission strengths as an estimate of sample contamination by field stars.

When combined with previously identified, higher mass stars, this search provides a sensitive measurement of the stellar mass function and dynamical structure of the Pleiades. The degree of tidal elongation of the halo agrees well with current N body simulation results. Tidal truncation affects masses below $\sim 1 M_\odot$. The cluster contains a total mass $\sim 800 M_\odot$. Evidence for a flatter mass function in the core than in the halo indicates the depletion of stars in the core with mass less than $\sim 0.5 M_\odot$, relative to stars with mass $\sim 1 - 0.5 M_\odot$, and implies a preference for very low mass objects to populate the halo or escape. The overall mass function is best fitted with a lognormal form that becomes flat at $\sim 0.1 M_\odot$. Whether sufficient dynamical evaporation has occurred to detectably flatten the initial mass function, via preferential escape of very low mass stars and brown dwarfs, is undetermined, pending better membership information for stars at large radial distances.

Subject headings: open clusters and associations: Pleiades, stars: low mass, brown dwarfs, astrometry, celestial mechanics, stellar dynamics

1. INTRODUCTION

The age distribution of open clusters suggests they are transient objects which are dissolved by the Galactic tidal field in time scales typically less than ~ 1 Gyr (Wielen 1971). Due to their small number of constituent stars, open clusters have short relaxation times of order 10^8 years or less, comparable to their typical crossing time, and can thus be understood only as collisional systems which evolve rapidly compared to larger systems, such as globular clusters (King 1980). This rapid evolution produces observable effects, such as mass segregation and the development of a halo, where tidal forces cause the dispersal of escaping stars. Despite the theoretical problems associated with collisional systems, the small number density of stars in open clusters allows the use of direct N body simulation as a practical tool of study (eg. Terlevich 1987; Kroupa 1995; Aarseth 1999; Portegies Zwart 2000). Unfortunately, N body simulations have suffered from a lack of detailed observational guidance.

The Pleiades cluster represents an appropriate laboratory for stellar dynamics – bright and rich in stars, but old enough to be dynamically evolved. Studies of the Pleiades date back to Trumpler (1920) and Hertzsprung (1947) (HII), and include those of Jones (1981), Haro, Chavira, & Gonzalez (1982) (HCG), van Leeuwen (1983), Stauffer et al. (1991) (SK), Rosvick, Mermilliod

& Mayor (1992), and Schilbach et al. (1995). The last large, faint proper motion survey was that of Hambly, Hawkins, & Jameson (1993) (HHJ) which revealed 440 probable members in 25 square degrees around the cluster center. Although the HHJ survey discovered many low mass cluster members, it was spatially incomplete, and the authors suggested that a larger survey would be fruitful. Research groups during the last decade have conducted many deep photometric searches for brown dwarfs in small fields aimed at studying the substellar mass function, such as Stauffer et al. (1989); Stauffer, Hamilton, & Probst (1994); Zapatero Osorio, Rebolo, & Martín (1997); Bouvier et al. (1998), and Festin (1998). Most have concluded that brown dwarfs are abundant in the Pleiades, but not numerous enough to contribute significantly to the total cluster mass. Observations of lithium absorption in brown dwarfs has lead to a precise age measurement for the Pleiades of 120 Myr (Stauffer, Schultz, & Kirkpatrick 1998), a result which has interesting implications for the dynamical state of the cluster as well as stellar astrophysics.

Despite a rich history of vigorous research in the Pleiades, the spatial incompleteness of previous surveys leaves some basic but critical properties of the cluster poorly constrained, such as its overall extent, structure, mass function and total mass. This paper summarizes the results of a spatially complete photometric and proper motion search in the Pleiades using the Two Micron All Sky Survey (2MASS) and proper motions determined from First Palomar Observatory Sky Survey (POSS I) plates and the Second Palomar Observatory Sky Survey (POSS II) (Reid et al. 1991) plates. Our primary goal is to characterize the fundamental structure of the Pleiades and estimate the mass function below $0.5 M_{\odot}$ to the completeness of the POSS *E* plates, roughly $0.1 M_{\odot}$ for cluster members.

2. DATA

This study used 2MASS point source data in the Pleiades field, which provided JHK_s photometry and positions on a uniform reference frame, and also indicated the presence of any optical counterpart in the USNO-A catalog (Monet et al. 1996). The 2MASS data exceeded a signal-to-noise ratio of 10 at $J = 15.8$, $H = 15.1$, and $K_s = 14.3$. The Pleiades area covered a 10° radius around the nominal center of RA = $3^{\text{h}}47^{\text{m}}$, DEC = $24^{\circ}7'$ (Lyngå 1987). 2MASS detected $\sim 7.8 \times 10^5$ sources in JHK_s in the field down to $K_s = 15$ (compare with several hundred known Pleiades members).

The USNO's Precision Measuring Machine (PMM) program (Monet 1998) scanned and digitized POSS I *E* plates and POSS II *F* plates. The PMM detections provided first and second epoch point source positions and instrumental R_E and R_F magnitudes. Errors in positions and magnitudes should be comparable to the USNO-A catalog, about $0.25''$ and 0.25 magnitudes respectively, in the magnitude range 12 – 19 (Monet et al. 1996). The ~ 35 year baseline between POSS I and POSS II allowed proper motion measurements to distinguish faint, red Pleiades candidates from field stars. We correlated *E* and *F* detections in the Pleiades field using a $5''$ search radius over roughly a 10° radius around the nominal cluster center. Before computing proper motions,

we attempted a first-order correction for systematic dispersion of the POSS I - POSS II positional offsets over large plate areas and across plate boundaries by subtracting the mean positional offsets between POSS I and POSS II counterparts brighter than $R_E = 18$ in $10' \times 10'$ boxes. A correlation of POSS sources with 2MASS JHK_s detections produced a database of $\sim 6.3 \times 10^5$ sources with 2MASS positions, $R_E R_F JHK$ magnitudes, and relative proper motions. The correlation with 2MASS and the five band detection requirement ensures that the database contains few spurious sources.

3. CLUSTER EXTRACTION

3.1. Color selection

Even in proper motion space the large area of this Pleiades search introduces a substantial amount of field star contamination. To reduce this contamination, a broad color filter selected only sources with colors similar to known Pleiades members. We chose to include sources in the range $8.0 \leq K_s \leq 14.75$ based on the dynamic range of the PMM extractions at the bright end and by the sensitivity of the POSS plates at the faint end. The color filter included the faint portion of the Pleiades locus, in the range $10 \leq K_s \leq 14$, composed mainly of late K and early to mid-M dwarfs. We extended the faint end of the magnitude range beyond $K_s = 14$ to try to include objects near the hydrogen burning limit at $K_s \approx 14.5$. Figures 1 and 2 show the specific location of color selection in the K_s vs. $R_E - K_s$ and $J - K_s$ color-magnitude diagrams, respectively. We deliberately chose broad regions to account for dispersion due to photometric error at faint magnitudes, as well as binarity. For sources fainter than $K_s = 14$, we excluded 2MASS sources that have a USNO-A counterpart in the 2MASS database, since faint, red Pleiades members will likely be absent in the blue-limited USNO-A catalog. In total, ~ 38000 sources to $K_s = 14$ and ~ 5700 sources fainter than $K_s = 14$ survived the color selection. In Figure 3, the density of points in a vector point diagram (VPD) for these color-selected stars reveals the cluster in proper motion space, as well as the still-dominant field star population. The proper motion dispersion due to internal dispersion in velocities, ~ 0.5 km/s (Jones 1970), is negligible compared with the uncertainty in the astrometry.

3.2. Membership probability

The color cuts sufficiently reduce the density of field-to-cluster sources in proper motion space to allow the computation of relative membership probabilities p given by

$$p = \frac{\Phi_c}{\Phi_c + \Phi_f}$$

where Φ_c and Φ_f are the distribution functions for the cluster and field stars respectively in the VPD. We fitted the distribution functions using a modified version of the maximum likelihood

technique of Sanders (1971). The distribution functions resembled those discussed in detail by Jones & Stauffer (1991), ie., a bivariate gaussian for the cluster, and an exponential distribution along the cluster’s mean proper motion with a gaussian in the orthogonal direction for the field. However, we chose not to include radial distance from the center of the cluster as a variable parameter in the distribution function in order to measure the true cluster extent free of model bias and to estimate the surface density of non-member stars with coincidentally high membership probabilities at large radial distance.

The distribution function fitting procedure operated on ~ 5600 sources contained in a region approximately 5×5 "/cent. around the cluster centroid. Due to the large number of field stars in the region, we found fitting the distribution functions in small magnitude groups difficult, particularly for faint stars. We fitted the distribution function without a magnitude dependence. This will affect the membership probabilities by favoring parameters that best fit the magnitudes with the least field contamination. However, the effect should be small except at the faint end of the sample. Membership probabilities for the ~ 500 sources fainter than about $K_s = 14$ are much less reliable than those for the the relatively brighter stars for two reasons. First, degradation in the PMM astrometry at faint magnitudes causes a larger dispersion in proper motion space, which makes modelling their distribution difficult. The faint clusters members are dispersed to smaller membership probabilities than relatively brighter cluster members. Second, field contamination increases at faint magnitudes. Membership of candidates fainter than about $K_s \approx 14$ will thus rely more heavily on their spectral properties.

The large area covered by this work results in enough field contamination to numerically dilute the membership probabilities. However, Figure 4 shows that most sources with $p > 0.3$ are likely to be cluster members based on the overall distribution of probabilities. The spatial distribution of sources with membership probability depicted in Figure 5 demonstrates qualitative statistical consistency of proper motion membership probability with true association with the cluster.

4. SPECTROSCOPY

In order to determine the success of the proper motion search, and estimate the field star contamination in our sample, we obtained optical spectra for a large number of our Pleiades candidates. M dwarf members of the Pleiades exhibit strong chromospheric activity (Prosser, Stauffer, & Kraft 1991; Steele & Jameson 1995), detectable through resulting $H\alpha$ emission, while field M dwarfs are usually less active (Hawley, Gizis, & Reid 1996). Therefore, absence of $H\alpha$ emission distinguishes obvious field stars from Pleiades members.

The spectra were taken using the Hydra red cable fiber-fed spectrograph and T2K CCD camera at the WIYN telescope⁴ (Barden et al. 1994) at Kitt Peak National Observatory during November

⁴The WIYN Observatory is a joint facility of the University of Wisconsin-Madison, Indiana University, Yale

25-28, 1999. The spectrograph was configured with the 600@13.9 grating in the 6200 - 8900 Å wavelength region for a dispersion of about 1.4 Å/pixel. While most spectroscopic fields fell within 2° of the cluster center, we targeted several fields at larger radial distance. Table 1 lists the positions of the centers of the WIYN Hydra fields, each approximately 1° in diameter, along with the number of candidates and control stars observed, and total exposure time used in each field. Fields near the center of the cluster partially overlapped so that about 128 candidates were observed more than once. The observations included 121 control targets with colors similar to the Pleiades candidates but that were expected to be field stars based on having proper motion farther than 3"/cent. from the cluster centroid in the VPD.

We used standard CCD reductions and analysis routines in IRAF⁵, and subsequently measured the equivalent width of H α line ($W_{H\alpha}$) from each one-dimensional spectrum using the FITPROFS routine over a spectral region of 6555–6569 Å. For candidates observed more than once, we averaged the individual $W_{H\alpha}$ measurements. Figure 6 displays a small sample of spectra for candidates with H α emission.

Figure 7 shows the distribution of $W_{H\alpha}$ for the 528 Pleiades candidates as well as the 121 control sources in the spectroscopic study. The shaded region indicates our $W_{H\alpha}$ measurement for previously known members in the sample. A χ^2 test suggests there is less than 10⁻⁵ probability that the candidate sample and the control sample are derived from the same distribution function. However, about 75 Pleiades candidates in the spectroscopic sample do not show strong H α emission, indicating that a fraction of our overall sample contains field stars.

5. MEMBERSHIP LIST

In total, this Pleiades search has identified 4233 possible Pleiades members with $p \geq 0.01$. Most will actually be non-members at large radial distances. Roughly 1200 are high probability members with $p \geq 0.3$ within a 6° distance from the cluster center.

5.1. Contamination

Table 2 shows the statistical dependence of $W_{H\alpha}$ with respect to proper motion membership probability, K_s magnitude, and radial distance. As expected, the contamination is worst at large radial distance and at faint magnitudes. For sources with $p \geq 0.01$ in the magnitude range $11 \leq K_s \leq 14$ within 5° of the cluster center, we estimate the overall contamination to be about 13%. The

University, and the National Optical Astronomy Observatories.

⁵IRAF is distributed by the National Optical Astronomy Observatories, which is operated by the Association of Universities for Research in Astronomy, Inc., under contract with the National Science Foundation.

lower surface density of field stars at relatively brighter magnitudes implies a lower contamination level for brighter stars. Outside a 5° radius, we expect the contamination to dominate the sample, but cannot yet quantify it without individual membership information obtained, for example, from radial velocity measurements.

The sample of 121 field stars contained 104 M dwarfs that had spectral types similar to the Pleiades candidates, M2 – M6 (Adams 2000). Among these 104 objects, 29 had $W_{H\alpha} > 1 \text{ \AA}$, and 18 had $W_{H\alpha} > 3 \text{ \AA}$. Assuming that stars with $W_{H\alpha} > 1 \text{ \AA}$ are indeed dMe stars, the 28% dMe rate in the M2 – M6 range agrees well with the data given in Hawley, Gizis, & Reid (1996), although the Pleiades field sample is too small to determine the dMe fraction as a function of spectral type. Thus, from the 70 Pleiades candidates in the range M2 – M6 that we assume are not members ($W_{H\alpha} < 1 \text{ \AA}$), we can estimate roughly 27 dMe stars in the sample of 434 with $W_{H\alpha} > 1 \text{ \AA}$, or 6% dMe contamination.

5.2. Completeness and sensitivity

The dynamic range of the PMM extractions limits the completeness at the bright end of this search. Counts for sources with correlated $R_E R_F JHK_s$ detections indicate that the PMM detections are complete up to $R \approx 8$, corresponding to $\sim 1.5 M_\odot$ for Pleiades members. Since our primary goal is to detect low mass stars, incompleteness at the bright end of our sample should not pose a significant problem due to the large amount of published data for bright Pleiades members.

This work recovered over 92% of the HHJ sample including several of their faintest objects, such as HHJ 3 and HHJ 2 (albeit at relatively low membership probability), indicating that it is relatively complete to $R = 19$. This work has also discovered about 269 candidates with $p \geq 0.3$ that were in the HHJ survey area but not in their list. Spectra for 109 of these candidates show that 83% have $W_{H\alpha}$ consistent with cluster membership ($3 - 14 \text{ \AA}$), while 94% of HHJ stars in our list have $W_{H\alpha}$ consistent with cluster membership. Thus, while our study appears to be more complete than HHJ, it is also more contaminated. If 83% of the 269 new objects in the HHJ and region and sensitivity range are in fact Pleiades members, then the HHJ survey is 66% complete relative to a projected total of 663 objects, in good agreement with their completeness estimation of 70% through most of their sensitivity range.

This search also recovered 8 objects from the survey of Bouvier et al. (1998), including CFHT-PL-5 and CFHT-PL-10, 3 PPI objects from Stauffer et al. (1989) including PPI 13, and no objects from Zapatero Osorio, Rebolo, & Martín (1997). Thus it is very incomplete at the hydrogen burning limit, $R = 20$ (Stauffer, Schultz, & Kirkpatrick 1998), and below.

5.3. Merging Pleiades catalogs

In order to construct a “complete” Pleiades catalog containing faint stars from this work and brighter stars from previous work, we merged our list of Pleiades candidates with probable members contained in the CfA Open Cluster Database⁶, derived primarily from HII, SK, HCG, and HHJ. We did not merge our list with any other external catalogs containing members brighter than our sample, since most are spatially incomplete.

For this study, approximate masses are suitable for dividing all Pleiades candidates into dynamical mass groups. Adjustment of apparent magnitudes, using a distance modulus of 5.5 (Lyngå 1987), yielded absolute magnitudes. Interpolation of mass-luminosity relations from Baraffe et al. (1998) provided masses for the candidates detected in this study, using 2MASS J magnitudes or HHJ I magnitudes for a few HHJ stars not recovered. Mass- M_V relations from Henry & McCarthy (1993) for $M_V \geq 1.45$, and Allen (1973) for $M_V < 1.45$, converted V magnitudes into masses for stars in the CfA Open Cluster Database. Variations between photometric systems of the mass-luminosity relations and the data will not affect the stellar mass estimates appreciably.

6. RESULTS AND DISCUSSION

6.1. Mass segregation and the mass function

6.1.1. Internal Structure

The long term internal evolution of an open cluster is described in terms of energy equipartition from kinetic theory of collisional systems. Briefly, lower mass stars, through encounters with high mass stars and binaries systems, acquire higher velocities resulting in larger, more radial orbits. High mass stars lose velocity and thus rapidly “sink” to the center of the cluster, where they can form binaries which become tighter, or disrupt, as a result of the encounters in the core. Mass segregation has been discussed by Spitzer & Shull (1975), and verified by the N body simulations of Terlevich (1987) and Kroupa (1995). This section discusses radial distribution of mass in the Pleiades, emphasizing stars with mass less than $1 M_\odot$.

To estimate the extent of the cluster on the sky, we divided Pleiades candidates with $p \geq 0.3$ into high ($\geq 2 M_\odot$), intermediate ($1 - 2 M_\odot$), and low ($< 1 M_\odot$) mass groups and then binned the high mass stars into 0.25° annuli, and the low and intermediate mass stars into 0.5° annuli. Figure 8 shows the radial distribution of surface number density for the three mass groups out to a radius $r \approx 10^\circ$ from the cluster center. The low mass group clearly fits a standard, three-parameter, single-mass King model (King 1962). Subtraction of the mean background surface number density,

⁶Provided by C.F. Prosser (deceased) and J.R. Stauffer, and which currently may be accessed at <http://cfa-ftp.harvard.edu/stauffer/>, or by anonymous ftp to [cfa-ftp.harvard.edu, cd /pub/stauffer/clusters/](ftp://cfa-ftp.harvard.edu/cd/pub/stauffer/clusters/)

determined in the annulus at $7 - 10^\circ$, from each annulus yielded an estimate of the cluster surface number density. The best chi-square fit gave a core radius $r_c = 1.0^\circ - 1.3^\circ$ and King tidal radius $r_t = 5.8^\circ - 6.8^\circ$ at 99% confidence. Figure 8 shows this fit superimposed on the mean background surface density. Note that these numbers only parameterize the empirical distribution of low mass stars on the sky, and this King tidal radius does not necessarily correspond to the location of the cluster’s Lagrangian points along the Galactic X direction. Since the cluster’s location is $l = 166^\circ$ and $b = -23^\circ$, the Lagrangian points in the X direction lie nearly along the line of sight, projected near the dense cluster center.

A King model allows an estimate of the spatial number density $\phi(r)$ within the cluster. The surface density in eq. (25) of King (1962) was differentiated numerically. Figure 9 shows the resulting spatial densities of mass groups with the low mass stars subdivided into finer mass groups, for stars with $p \geq 0.3$, and assuming a distance modulus of 5.5 (Lyngå 1987). The highest mass stars dominate the core in terms of mass density, while stars below $1 M_\odot$ dominate the halo beyond ~ 5 pc. This classical effect of mass segregation has been well established in the Pleiades and other clusters (eg. van Leeuwen 1983; Hambly et al. 1995; Raboud & Mermilliod 1998b), and confirms high mass stars in the core are much closer to energy equipartition than stars in the halo (Giersz & Heggie 1996; 1997). Stars with masses less than $1 M_\odot$ have similar radial extent, implying tidal truncation affects stars with mass up to $\sim 1 M_\odot$. This result indicates that relatively bright stars up to $V \approx 12$ can be used to trace escape processes around the cluster using upcoming high precision, space-based astrometry missions such as FAME (Horner et al. 1999) or SIM (Unwin 1999), which, according to specifications, should constrain nearly the entire phase space for detected stars in nearby clusters such as the Pleiades.

The dynamics that drive mass segregation can deplete low mass objects in the core. Simulations (eg. Terlevich 1987) predict spatial variations in the mass function during core contraction and formation of an extended halo dominated by low mass stars. Terlevich’s results show a relatively smaller ratio of $0.3 M_\odot$ stars to $0.8 M_\odot$ stars in the core than in the halo. Thus, migration from the core can occur preferentially for stars with mass less than the average stellar mass in clusters, flattening the slope of the observed mass function at low mass.

To look for this effect, we calculated the mass function $\Psi(m)$, where

$$\Psi(m) = \frac{dN}{dm}$$

represents the distribution of mass in terms of the number of stars N in the mass interval $[m, m + dm]$. Because field star contamination increases with radial distance and may pollute the observed mass function, we attempted to statistically subtract field contamination. We scaled the number of field stars in each mass bin per unit area in the annulus at $6.5^\circ - 9.0^\circ$ for the corresponding area covered by each mass function, and subsequently subtracted the expected number of field stars from each mass bin. Figure 10 shows the dependence of the mass function on radial distance for stars with mass $1 - 0.1 M_\odot$ and $p \geq 0.3$, after field subtraction. The results show a more flattened mass function in the core. A chi-square test for binned data (Press et al. 1992) shows a significant

difference in the mass functions: there is 11% probability that the mass function within 1 core radius and 1 – 2 core radii represent the same distribution function, and 15% probability the mass function within 1 core radius and outside 2 core radii represent the same distribution function. For comparison, we performed a Kolmogorov-Smirnov test (Press et al. 1992) between the mass functions *before* binning and field subtraction. Results indicate 21% probability the mass function within 1 core radius and 1 – 2 core radii represent the same cumulative distribution function, and less than 1% probability the mass function within 1 core radius and outside 2 core radii represent the same cumulative distribution function.

The slightly flatter mass function in the Pleiades core suggests a marginal detection of preferential depletion of low mass objects at the center of the cluster. Moreover, projection of foreground halo stars onto the observed core means the mass function in the central part of the cluster may be more depleted of low mass objects than observed in projection. Tidal truncation below $\sim 1 M_{\odot}$ then implies slightly higher relative escape rates for stars below average mass, roughly 0.4 – 0.5 M_{\odot} . Preferential escape may affect the slope of the overall observed mass function, discussed next.

6.1.2. Overall mass function

The abundance of low mass stars in stellar systems makes them important players in dynamical processes. The character of the mass function (MF) in rich, young clusters such as the Pleiades has important ramifications for the initial mass function (IMF) in star formation, since most stars are believed to form in clusters (Lada, Strom, & Myers 1993). The MF is also a critical ingredient in N body simulations with implications for the internal dynamics of energy equipartition (eg. Inagaki & Saslaw 1985; Giersz & Heggie 1996) and expected lifetime of clusters (Terlevich 1987; de la Fuente Marcos 1995).

Figure 11 shows the distribution of Pleiades masses below 1 M_{\odot} for stars with $p \geq 0.3$ and radial distance less than 5.5° . Error bars portray Poisson statistics. The completeness of the sample begins to decrease below $\sim 0.15 M_{\odot}$. We agree with Hambly et al. (1999) that the Pleiades MF is best fit in $\log dN/dm$ vs. $\log m$ space with a log normal (quadratic) function rather than a single exponent power law. The best polynomial fit in the 1 – 0.1 M_{\odot} region gives

$$\log(N \text{ per } 0.1 M_{\odot} \text{ bin}) = -0.93 \pm 0.03(\log m)^2 - 1.86 \pm 0.02 \log m + 1.59 \pm 0.02$$

as delineated in Figure 11. The overall field star contamination in this sample is expected to be roughly 10 – 15% (or less for stars above 0.5 M_{\odot}). This amount of field star contamination should have little effect on the coefficients of the fit. Thus the Pleiades MF appears to be slowly rising below 0.5 M_{\odot} and relatively flat at 0.1 M_{\odot} . This MF could be considered a lower limit at the faint end due to incompleteness and unresolved binarity.

Although less steep in the 0.3 – 0.1 M_{\odot} region than those inferred by brown dwarf surveys (Bouvier et al. 1998; Hambly et al. 1999), this Pleiades MF appears consistent with previous

results, as shown in Figure 11, and suggests a flat or decreasing MF at the hydrogen burning limit. Assuming that this MF continues below $0.04 M_{\odot}$, the 303 objects in the lowest $0.1 M_{\odot}$ mass bin imply a *crude* lower limit of ~ 200 free-floating objects below the hydrogen burning mass limit at $0.075 M_{\odot}$. Unless the MF rises sharply below $0.06 M_{\odot}$, the total brown dwarf mass contribution is likely to be less than 5% of the total Pleiades mass.

For comparison, Figure 11 also shows power law functions, $\Psi(m) \propto m^{-\alpha}$, for a Salpeter MF ($\alpha = 2.35$) (Salpeter 1955) and for the local field MF ($\alpha = 1.05$) (Reid & Gizis 1997), normalized to $\sim 1 M_{\odot}$. While our MF alone is not necessarily inconsistent with $\alpha \approx 1$ at $0.15 M_{\odot}$ due to incompleteness and binarity (discussed below), our results combined with those of Bouvier et al. (1998) and Hambly et al. (1999) seem to show a persistent flattening below $0.2 M_{\odot}$, in contrast to the local field MF, which continues to rise to $0.1 M_{\odot}$.

A key question is whether the Pleiades MF represents initial conditions or dynamical evaporation. Substantial evaporation will flatten the present day MF from the IMF, since low mass objects escape preferentially. However, the Pleiades may have evaporated too few stars to alter the slope of the observed IMF at low mass. For example, de la Fuente Marcos & de la Fuente Marcos (2000) performed simulations which showed little fractional depletion of brown dwarfs, compared with stars, until cluster half-life. Without better membership information at large radial distances, and a reliable estimate of the number of escaped cluster members, we cannot quantify the precise degree of evolution the MF exhibits.

6.1.3. Unresolved binarity

Many Pleiades proper motion candidates are unresolved binaries that will systematically affect measurements of the mass function and total mass in stars. In order to derive a correction for unresolved binaries, we performed a simple simulation of the observed masses in a cluster with known primary mass function and frequency and mass distribution of binary companions. The simulation used standard Monte Carlo techniques, as well as the mass-luminosity relations mentioned in §5.3.

The primary mass distribution consisted of a generic log-normal MF. A binary frequency function $f(m)$, and a distribution of mass ratios $q(m) = m_2/m_1$ where m_1 is the primary mass and m_2 the secondary mass, determined secondary masses. The hypothetical cluster contained stars in high, medium, and low mass groups of $m/M_{\odot} \geq 2$; $1 \leq m/M_{\odot} < 2$; and $m/M_{\odot} < 1$, respectively.

Realistic values for $f(m)$ are 0.5 for the high and medium mass group and 0.3 for the low mass group (Abt & Levy 1976; Mermilliod et al. 1992). Input parameters for the mass function and q distribution were adopted from Duquennoy & Mayor (1991) and Kroupa, Tout, & Gilmore (1990). The primary masses were distributed in N (per unit $\log m$) – $\log m$ space with gaussian peak at $\log m \sim -0.5$ and width of ~ 0.4 . Since they are poorly determined, we varied the parameters of the MF distribution slightly during the simulations, typically by a couple of tenths in central value and width. The q distribution consisted of a gaussian with peak 0.23 and width 0.42. For stars

with mass lower than $1 M_{\odot}$, the q distribution was flattened, as suggested by data from Mermilliod et al. (1992).

Figure 12 shows a typical observed mass function for a given true mass function in $\log dN/dM - \log m$ space for a cluster containing 10000 stars. The observed mass function underestimates the true mass function below $0.5 M_{\odot}$ by a factor of 1 – 2 down to $0.1 M_{\odot}$. This simulation assumed that all Pleiades binaries were unresolved, since 2MASS spatially resolves only the widest binaries ($> 10^5$ AU) at the distance of the Pleiades. The simulations suggest that unresolved binaries at low mass may affect the slope of a mass function α by up to a few tenths below $0.5 M_{\odot}$. Repeated simulations determine an overall mass correction factor δ where $M_{true} = (1 + \delta)M_{obs}$. Computing the effective apparent magnitude for the binary stars, and integrating the true and observed mass functions to about $0.08 M_{\odot}$, gave $\delta \sim 0.15$. The simulations were most sensitive to $f(m)$. If $f(m) = 1$ for all masses, δ increases to ~ 0.3 . Sliding the peak of the mass function $0.2 \log m$ units resulted in a change in δ by about 0.02, where a higher peak causes a larger δ . A change the width of the mass function by $0.2 \log m$ units also resulted in a change in δ by about 0.02, where a wider mass function causes a larger δ . Note that δ was similar for repeated simulations of a cluster of 1000 stars.

This simulation is obviously crude, and eg. SIRTf observations would better determine Pleiades binarity at low mass.

6.2. Dynamical mass

A simple sum of the masses of individual members yields the total Pleiades mass. Candidates in the merged sample with $p \geq 0.3$ within a 5.5° radial distance from the nominal center are the most probable members. Integration of the individual masses to $0.1 M_{\odot}$ gives a total mass of $690 M_{\odot}$ and a binary-corrected mass of $\sim 800 M_{\odot}$. This simple sum contains systematic and random errors from field contamination, unresolved binaries, Poisson uncertainties, and completeness. Objects below $0.1 M_{\odot}$ are not likely to add more than a few percent to this mass estimate.

For a local Galactic cluster in circular orbit, the approximate limiting tidal radius r_{lim} for a member star along the direction towards or away from the Galactic center depends on the cluster mass M_c and the Galactic rotation curve (King 1962):

$$r_{lim} = \left[\frac{GM_c}{4A(A - B)} \right]^{\frac{1}{3}}$$

where A and B are the Oort constants. The values $A = 14.4 \text{ km s}^{-1} \text{ kpc}^{-1}$ and $B = -12.0 \text{ km s}^{-1} \text{ kpc}^{-1}$ (Kerr & Lynden-Bell 1986) correspond to a tidal radius of 13.1 pc, which confirms earlier results found by Pinfield, Jameson & Hodgkin (1998) using several different Pleiades catalogs and an expression for the tidal radius of a cluster in radial orbit (von Hoerner 1957). Figure 13 displays a projection of this radius. The tidal radius overlaps with the confidence interval for the “edge” of the

cluster determined from the King profile fit (Figure 8). Therefore, the limited size of the Pleiades indicates the absence of a massive population of brown dwarfs or internal dark matter. Thus we conclude that the stellar mass composes nearly the entire dynamical mass. Further comparison of r_{lim} given above with the King tidal radius r_t is dangerous as they represent different quantities in this case, since the direction of r_{lim} lies along the line of sight.

6.3. Projected halo structure

N body models predict an elongation of open clusters in roughly the X -direction and to a slightly lesser extent in the Y -direction, due to heating in the halo by the Galactic tidal field (Terlevich 1987; Portegies Zwart 2000). The tidal field in these models, generated from a circular cluster orbit in the Galactic plane, produces a nonspherical tidal surface resulting in a flattened structure with axial ratios 2:1.4:1 in the $X:Y:Z$ directions, respectively (Wielen 1975; Aarseth 1973). Terlevich predicts a fairly constant number of stars trapped in the halo, between 1 and 2 tidal radii, for some period of time before escaping permanently. Portegies Zwart maps escaping stars exiting primarily through the first and second Lagrangian points.

At $l = 166^\circ$ and $b = -23$, the projection of the Pleiades onto the sky is most sensitive to structure in the YZ plane. Following Raboud & Mermilliod (1998a), we used moment analysis to determine the ellipticity $e = (1 - b/a)$ of the Pleiades. This method allows direct, quantitative comparison of the Pleiades to a simulated cluster. Figure 14 shows measurements of e within a given radius r for Pleiades stars with mass $1 - 0.1 M_\odot$, with propagation of Poisson uncertainties determining the error bars. Field contamination dilutes the measured ellipticity, especially near and beyond the tidal radius at $\sim 6^\circ$. For comparison, Figure 14 also shows the ellipticity of Portegies Zwart’s (2000) models W4-III and W6-III at an age of 100 Myr. The W4 and W6 simulated clusters orbit at 6 kpc and 12 kpc, respectively, from the Galactic center. To compare their ellipticities with the Pleiades, we projected the positions of stars with mass $1 - 0.1 M_\odot$ to the location and size of the Pleiades on the sky, assuming binaries are unresolved. The models show similarity to the flattened structure throughout most of the Pleiades halo. The moment analysis confirms elongation in both the Pleiades and the models lies nearly parallel the Galactic plane; the major axes of the halos of the Pleiades and models lie consistently within 10° of the longitude of the cluster. However, the orientation of the ellipticity in the core of the Pleiades deviates more randomly from the halo by as much as 30° , suggesting the higher ellipticity in the Pleiades core seen in Figure 14 is probably due to coincidental projection effects rather than a consistent elliptical distribution, and thus is not physically significant. Clearly, better membership information is required for the outermost Pleiades stars. However, the models appear to adequately describe a young, but dynamically evolved, open cluster such as the Pleiades.

The Pleiades cluster has interacted with local environmental features not specifically included in the models. For example, the Pleiades probably migrated from the Sagittarius arm (Yuan & Waxman 1977). However, this would have occurred more than one relaxation time interval (~ 50

Myr) in the past, so the cluster, through evolution, has likely “forgotten” any effects from its passage out of the arm. Recent observations of interstellar gas in the vicinity of the Pleiades suggests that the cluster is coincidentally colliding with two small molecular clouds (eg. White & Bally 1993; White & Allen 1997) moving, relative to the Pleiades, at $\sim 15 - 20$ km/s. However, the mass of the gas is only $20 - 50 M_{\odot}$ (Bally & White 1986; Breger 1987), which is much smaller than the mass of the cluster stars. Thus, comparison of the Pleiades with models is legitimate since local features have had negligible effects on its present structure.

The Poisson statistics of the background stars in Figure 13 place an upper limit of ~ 1.7 stars deg^{-2} that may have escaped the Pleiades in the projected YZ plane. Without individual distance measurements, projection of the X direction along the line of sight prevents our probing the proposed escape mechanism near the Lagrangian points.

Since the Galactic tidal field is the primary catalyst for dispersal, a future measurement of the escape mechanism combined with structure and kinematic data in open clusters of various dynamical ages will better test our understanding of the nature of the tidal field. For example, substantial flattening has also been found in the Hyades (Oort 1979; Perryman et al. 1998) and Alpha Persei (Prosser 1992). However, other clusters, such as Praesepe (Raboud & Mermilliod 1998b) and M67 (Mathieu 1983), show less flattening. Better membership surveys are required in most clusters to study any dependence of structure on age or environmental effects. A comparison of the static tidal model results to those of more realistic simulations that include time dependent tidal fields from radial oscillation and vertical disk passage (eg. Murali & Weinberg 1997; Combes, Leon & Meylan 1999) would be a useful exercise to closely examine when the static approximation to the tidal field breaks down in clusters older than the Pleiades.

7. SUMMARY

This paper described a wide field proper motion search using 2MASS and PMM astrometry, which has detected ~ 1200 high probability, low mass Pleiades candidates, down to a mass $\sim 0.1 M_{\odot}$, from nearly 1 million stars in a 300 deg^2 field around the nominal center of the cluster. Several hundred are newly detected candidates. Spectroscopic results for 528 Pleiades candidates show a slight degree of contamination for high probability candidates to a radial distance of $\sim 5^{\circ}$. Beyond this distance, nearly all objects detected as Pleiades candidates are expected to be field stars.

The high mass cluster members are centrally concentrated with respect to low mass members. Tidal truncation is relevant to all objects with mass less than $\sim 1 M_{\odot}$. The mass function in the range $1 - 0.1 M_{\odot}$ is marginally flatter within the core than outside, indicating evidence for preferential escape of stars with less than average mass. These results agree with theoretical and numerical expectations.

The Pleiades mass function rises slowly below $1 M_{\odot}$ and appears to become flat at $0.1 M_{\odot}$, suggesting a lower limit of ~ 200 brown dwarfs in the cluster. This result is consistent with previous

surveys that conclude brown dwarfs contribute little to the dynamical mass. Stars with mass $1 - 0.1 M_{\odot}$ dominate the total mass. Better membership information, near and beyond the tidal radius, is needed to determine whether the Pleiades mass function represents the initial mass function, or reflects preferential evaporation of low mass objects. The total Pleiades stellar mass is $\sim 800 M_{\odot}$, including a 15% correction for unresolved binaries. The corresponding tidal radius to this mass estimate is approximately 13.1 pc. The apparent size of the Pleiades rules out a significant addition to this mass estimate from brown dwarfs or dark matter.

The cluster is highly flattened in the YZ plane, in good agreement with recent numerical models. This result confirms that the Galactic tidal field plays the dominant role in open cluster dispersal. Detection of the escape mechanism and dispersal rate will likely rely on future high precision, space-based astrometry.

We thank R. Cutri for assistance with 2MASS point source files for the Pleiades field. J. A. gratefully acknowledges S. Portegies Zwart for sharing and discussing simulation results. M. Weinberg and R. White provided helpful criticism for parts of this manuscript. NOAO funds for graduate student thesis observations provided travel support for J. A. This publication makes use of data products from the Two Micron All Sky Survey, which is a joint project of the University of Massachusetts and the Infrared Processing and Analysis Center, funded by the National Aeronautics and Space Administration and the National Science Foundation. The National Geographic Society-Palomar Observatory Sky Atlas (POSS I) was made by the California Institute of Technology with grants from the National Geographic Society. The Second Palomar Observatory Sky Survey (POSS II) was made by the California Institute of Technology with funds from the National Science Foundation, the National Geographic Society, the Sloan Foundation, the Samuel Oschin Foundation, and the Eastman Kodak Corporation. This research made use of the Digitized Sky Survey. The Digitized Sky Survey was produced at the Space Telescope Science Institute under US government grant NAGW-2166. The images of these surveys are based on photographic data obtained using the Oschin Schmidt Telescope on Palomar Mountain and the UK Schmidt Telescope. The plates were processed into the present compressed digital form with the permission of these institutions. This research has made use of NASA's Astrophysics Data System Abstract Service.

REFERENCES

- Aarseth, S. J. 1973, *Vistas Astr.*, 15, 13
- Aarseth, S. J. 1999, *PASP*, 111, 1333
- Abt, H. A. & Levy, S. G. 1976, *ApJS*, 30, 273
- Adams, J. D. 2000, Ph.D. Dissertation, University of Massachusetts Amherst
- Allen, C. W. 1973, *Astrophysical Quantities*, London: Athlone Press
- Bally, J. & White, R. E. 1986, *NASA Summer School on Interstellar Processes*, NASA Technical Memorandum 88342
- Baraffe, I., Chabrier, G., Allard, F. and Hauschildt, P. H. 1998, *A&A*, 337, 403
- Barden, S. C., Armandroff, T., Muller, G., Rudeen, A. C., Lewis, J., & Groves, L. 1994, *SPIE*, 2198,87
- Bouvier, J., Stauffer, J. R., Martín, E. L., Barrado y Navascués, D., Wallace, B., & Bejar, V. J. S. 1998, *A&A*, 336, 490
- Breger, M. 1987, *ApJ*, 319, 754
- Combes, F., Leon, S. & Meylan, G. 1999, *A&A*, 352, 149
- Duquennoy, A. & Mayor, M. 1991, *A&A*, 248, 485
- Festin, L. 1998, *A&A*, 333, 497
- de la Fuente Marcos, R. 1995, *A&A*, 301, 407
- de la Fuente Marcos, R. & de la Fuente Marcos, C. 2000, *Ap&SS*, 271, 127
- Giersz, M. & Heggie, D. C. 1996, *MNRAS*, 279, 1037
- Giersz, M. & Heggie, D. C. 1997, *MNRAS*, 286, 709
- Hambly, N. C., Hawkins, M. R. S., & Jameson, R. F. 1993, *A&AS*, 100, 607
- Hambly, N. C., Steele, I. A., Hawkins, M. R. S., & Jameson, R. F. 1995, *MNRAS*, 273, 505
- Hambly, N. C., Hodgkin, S. T., Cossburn, M. R., & Jameson, R. F. 1999, *MNRAS*, 303, 835
- Haro, G., Chavira, E., & Gonzalez, G. 1982, *Boll. del Instituto de Tonantzintla*, 3, 3
- Hawley, S. L., Gizis, J. E., & Reid, I. N. 1996, *AJ*, 112, 2799
- Henry, T. J. & McCarthy, D. W., Jr. 1993, *AJ*, 106, 773

- Hertzsprung, E. 1947, *Ann. Sterrew. Leiden*, 3
- von Hoerner, S. 1957, *ApJ*, 125, 451
- Horner, S. D., Germain, M. E., Greene, T. P., Harris, F. H., Harris, H. C., Johnson, M. S., Johnston, K. J., Monet, D. G., Murison, M. A., Phillips, J. D., Reasenber, R. D., Seidelmann, P. K., Urban, S. E., & Vassar, R. H. 1999, *BAAS*, 195, 88.01
- Inagaki, S. & Saslaw, W. C. 1985, *ApJ*, 292, 339
- Jones, B. F. 1970, *AJ*, 75, 563
- Jones, B. F. 1981, *AJ*, 86, 290
- Jones, B. F. & Stauffer, J. R. 1991, *AJ*, 102, 1080
- Kerr, F. J. & Lynden-Bell, D. 1986, *MNRAS*, 221, 1023
- King, I. 1962, *AJ*, 67, 471
- King, I. 1980, *IAUS 85, Star Clusters*, Hesser, J. ed., Dordrecht: Reidel, 139
- Kroupa, P., Tout, C. A., & Gilmore, G. 1990, *MNRAS*, 244, 76
- Kroupa, P. 1995, *MNRAS*, 277, 1522
- Lada, E. A., Strom, K. M., & Myers, P. C. 1993, in Levy, E. & Lunine, J. eds. *Protostars and Planets III*, University of Arizona, p. 245
- van Leeuwen, F. 1983, Ph.D. dissertation, Leiden University
- Lyngå, G. 1987, *Catalogue of Open Cluster Data (5th Ed.)*, Lund Observatory
- Mathieu, R. D. 1983, Ph.D. Dissertation, University of California Berkeley
- Mermilliod, J.-C., Rosvick, J. M., Duquennoy, A., & Mayor, M. 1992, *A&A*, 265, 513
- Monet, D., Bird, A., Canzian, B., Harris, H., Reid, N., Rhodes, A., Sell, S., Ables, H., Dahn, C., Guetter, H., Henden, A., Leggett, S., Levison, H., Luginbuhl, C., Martini, J., Monet, A., Pier, J., Riepe, B., Stone, R., Vrba, F., Walker, R. 1996, *USNO-SA1.0*, (U.S. Naval Observatory, Washington DC).
- Monet, D. 1998, *Astrophysics and Algorithms: a DIMACS Workshop on Massive Astronomical Data Sets*, 2
- Murali, C. & Weinberg, M. D. 1997, *MNRAS*, 291, 717
- Oort, J. H. 1979, *A&A*, 78, 312

- Perryman, M. A. C., Brown, A. G. A., Lebreton, Y., Gomez, A., Turon, C., de Strobel, G. C., Mermilliod, J. C., Robichon, N., Kovalesky, J., & Crifo, F. 1998, *A&A*, 331, 81
- Pinfield, D. J., Jameson, R. F., & Hodgkin, S. T. 1998, *MNRAS*, 299, 955
- Portegies Zwart, S. F. 2000, *MNRAS*, in press
- Press, W. H., Teukolsky, S. A., Vetterling, W. T. & Flannery, B. P. 1992, *Numerical Recipes in C*, Cambridge: Cambridge University Press
- Prosser, C. F., Stauffer, J. R., & Kraft, R. P. 1991, *AJ*, 101, 1361
- Prosser, C. F. 1992, *AJ*, 103, 488
- Raboud, D. & Mermilliod, J.-C. 1998a, *A&A*, 329, 101
- Raboud, D. & Mermilliod, J.-C. 1998b, *A&A*, 333, 897
- Reid, I. N., Brewer, C., Brucato, R. J., McKinley, W. R., Maury, A., Mendenhall, D., Mould, J. R., Mueller, J., Neugebauer, G., Phinney, J., Sargent, W. L. W., Schombert, J., & Thicksten, R. 1991, *PASP*, 103, 661
- Reid, I. N. & Gizis, J. E. 1997, *AJ*, 113, 2246
- Rosvick, J. M., Mermilliod, J.-C., & Mayor, M. 1992, *A&A*, 255, 130
- Salpeter, E. E. 1955, *ApJ*, 121, 161
- Sanders, W. L. 1971, *A&A*, 14, 226
- Schilbach, E., Robichon, N., Souchay J., and Guibert, J. 1995, *A&A*, 299, 696
- Spitzer, L. & Shull, J. M. 1975, *ApJ*, 201, 773
- Stauffer, J. R., Hamilton, D., Probst, R. G., Rieke, G., & Mateo, M. 1989, *ApJ*, 344L, 21
- Stauffer, J. R., Klemola, A., Prosser, C., & Probst, R. G. 1991, *AJ*, 101, 980
- Stauffer, J. R., Hamilton, D., & Probst, R. G. 1994, *AJ*, 108, 155
- Stauffer, J. R., Schultz, G., & Kirkpatrick, J. D. 1998, *ApJ*, 499L, 199
- Steele, I. A. & Jameson, R. F. 1995, *MNRAS*, 272, 630
- Terlevich, E. 1987, *MNRAS*, 224, 193
- Trumpler, R. J. 1920, *PASP*, 32, 43
- Unwin, S. C. 1999, *BAAS*, 195, 46.02

White, R. E. & Bally, J. 1993, *ApJ*, 409, 234

White, R. E. & Allen, C. L. 1997, submitted to *ApJ*

Wielen, R. 1971, *A&A*, 13, 309

Wielen, R. 1975, *IAUS 69, Dynamics of Stellar Systems*, Hayli, A. ed., Dordrecht: Reidel, 119

Yuan, C. & Waxman, A. M. 1977, *A&A*, 58, 65

Zapatero Osorio, M. R., Rebolo, R., & Martín, E. L. 1997, *A&A*, 317, 164

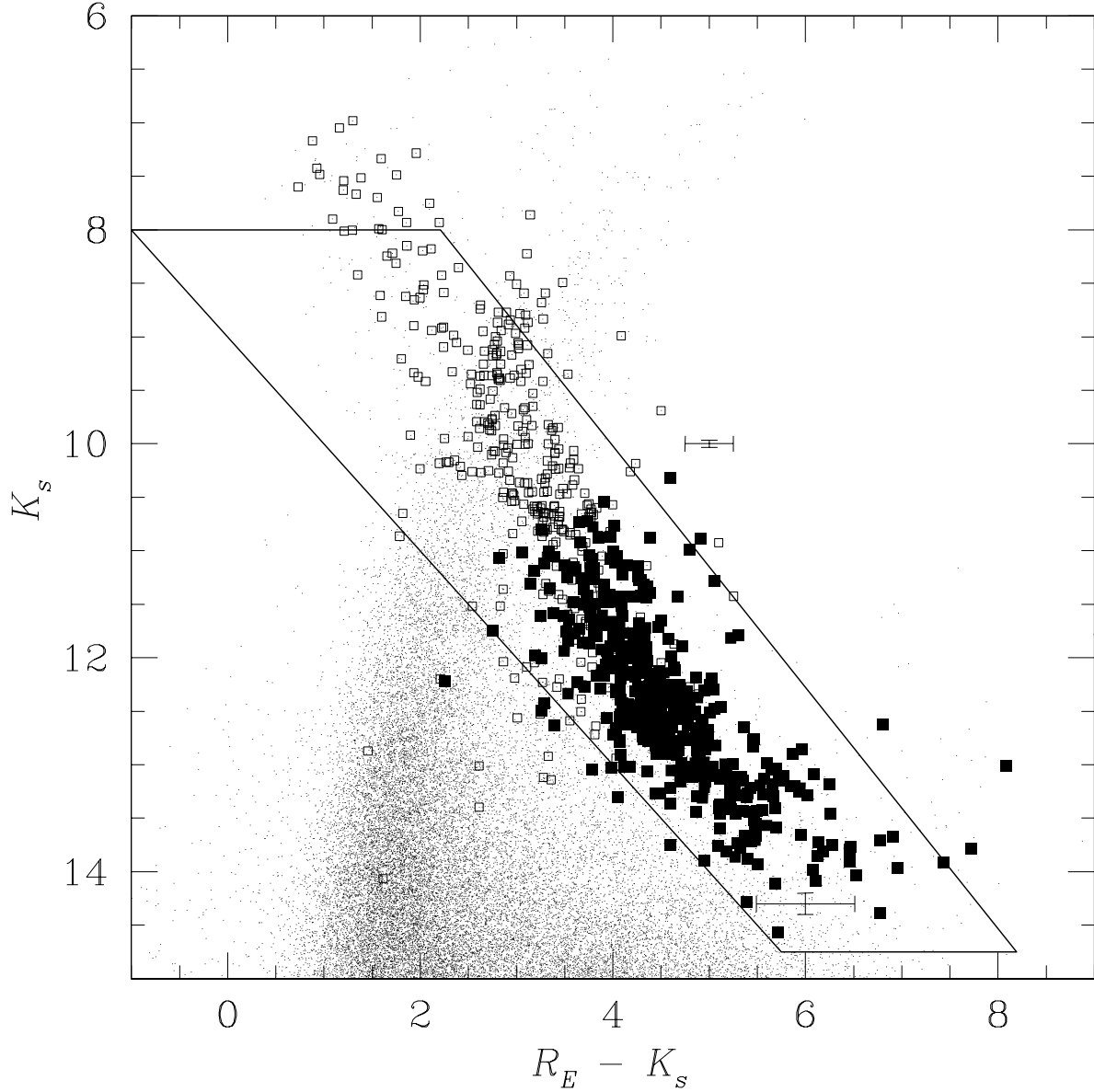


Fig. 1.— Color-magnitude diagram using instrumental R_E and 2MASS K_s magnitudes for field stars in a small area ($\sim 12 \text{ deg}^2$) around the Pleiades. The open squares represent colors for a sample of previously published Pleiades candidates brighter than the HHJ sample, while the solid squares represent colors for HHJ stars. Typical error bars are shown along the main sequence near $K_s = 10$ and $K_s = 14$. The boxed area indicates the region in which sources were selected for proper motion analysis.

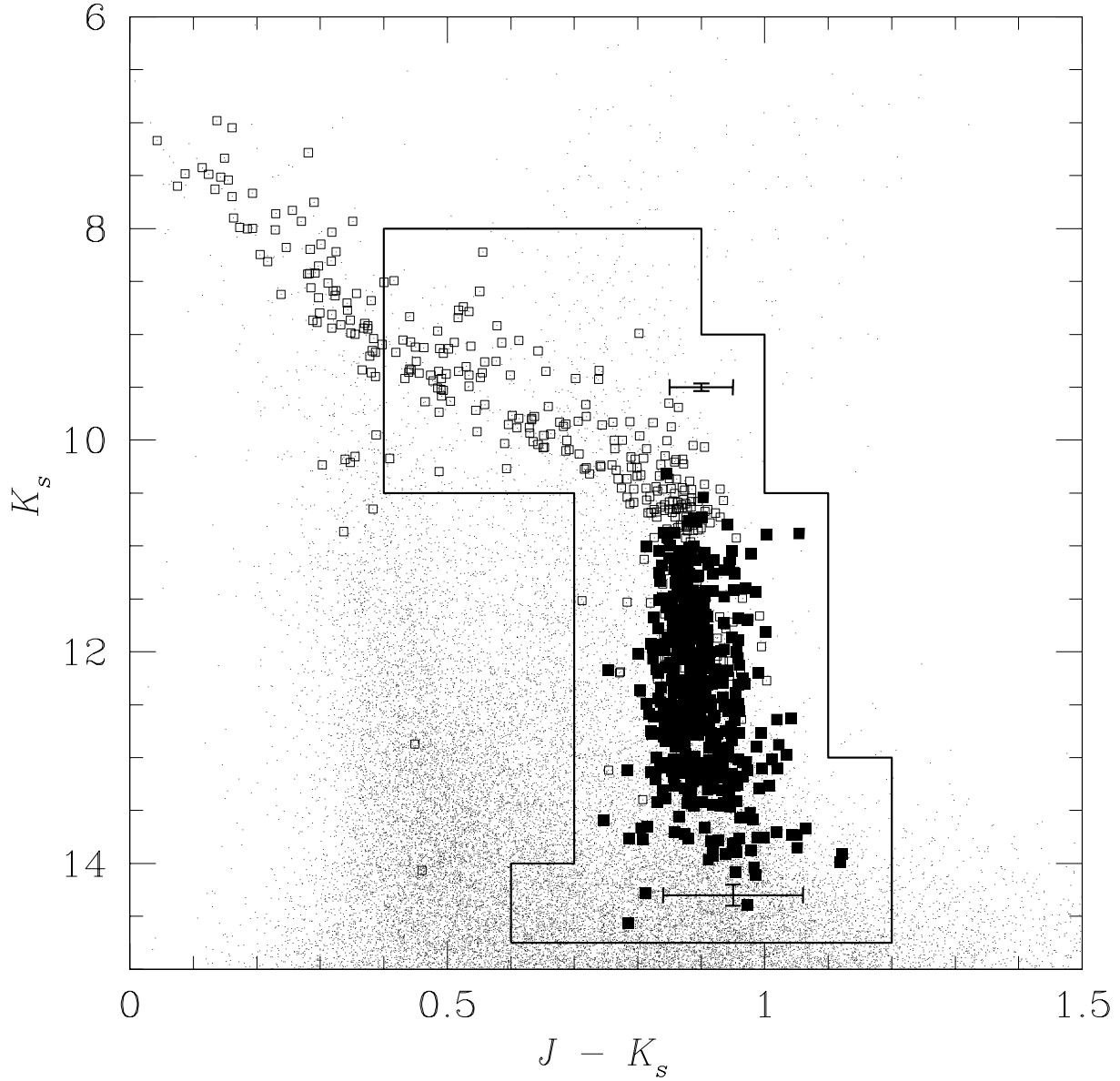


Fig. 2.— 2MASS $K_s : J - K_s$ color-magnitude diagram for the sources described in Figure 1. Symbols and boxed region analogous to those in Figure 1.

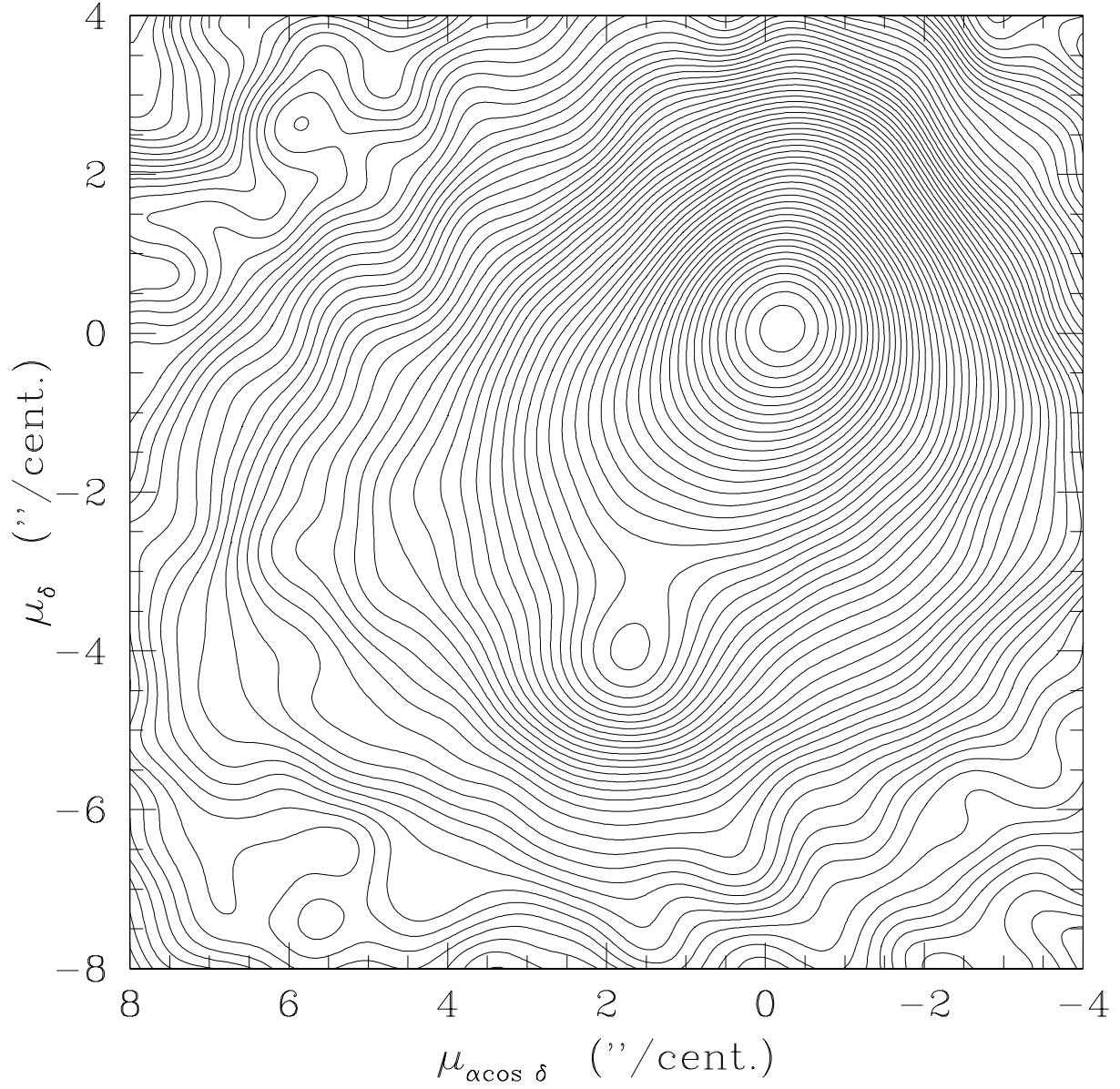


Fig. 3.— Contours derived from a Hess diagram of proper motion vectors, after color selection, for sources brighter than $K_s = 14$. The center of the field star distribution lies near (0,0) "/cent. and the cluster distribution is visible near (2,-4) "/cent.

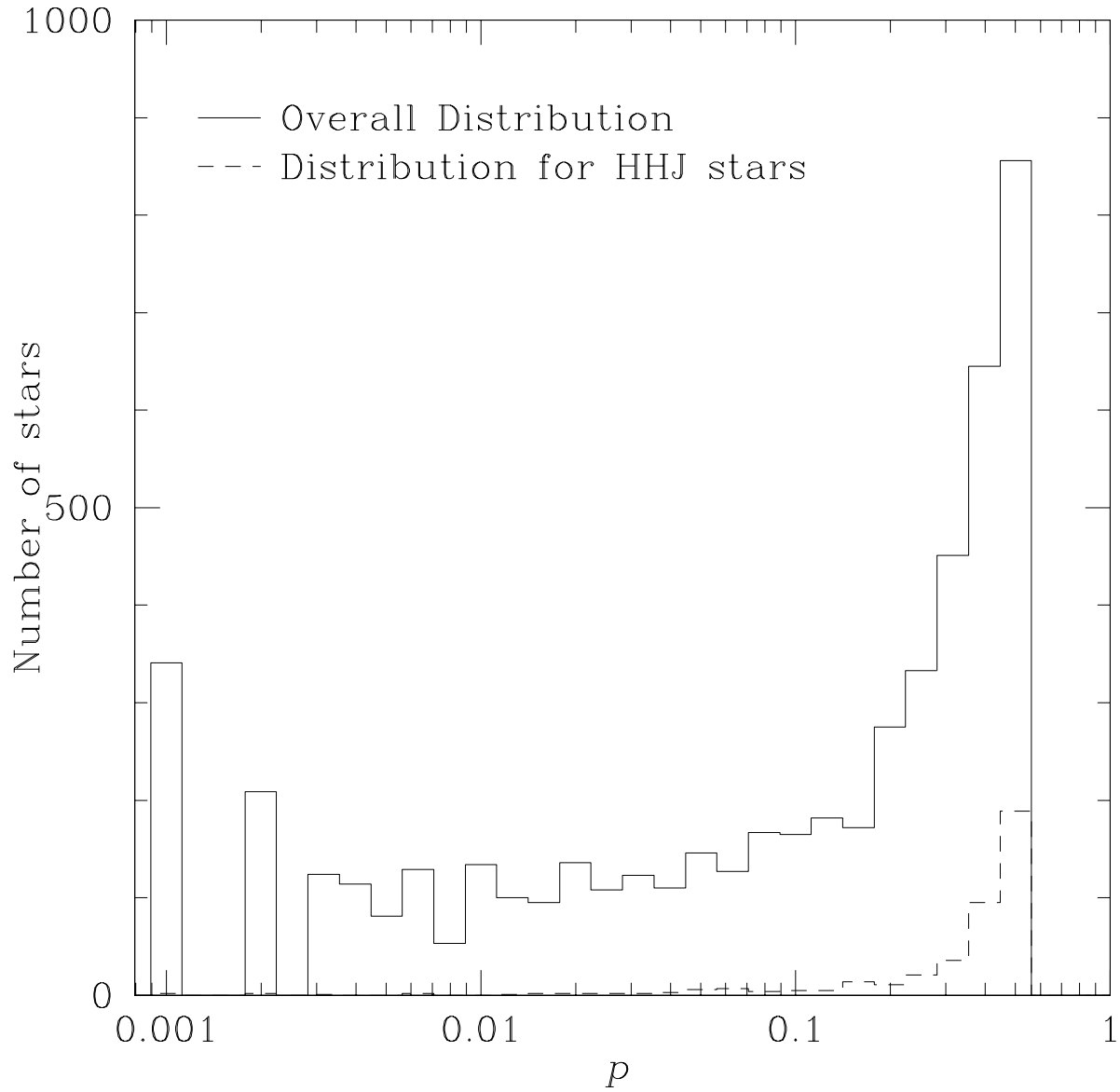


Fig. 4.— Distribution of membership probabilities p for Pleiades candidates. The dotted line shows the p distribution for recovered HHJ stars.

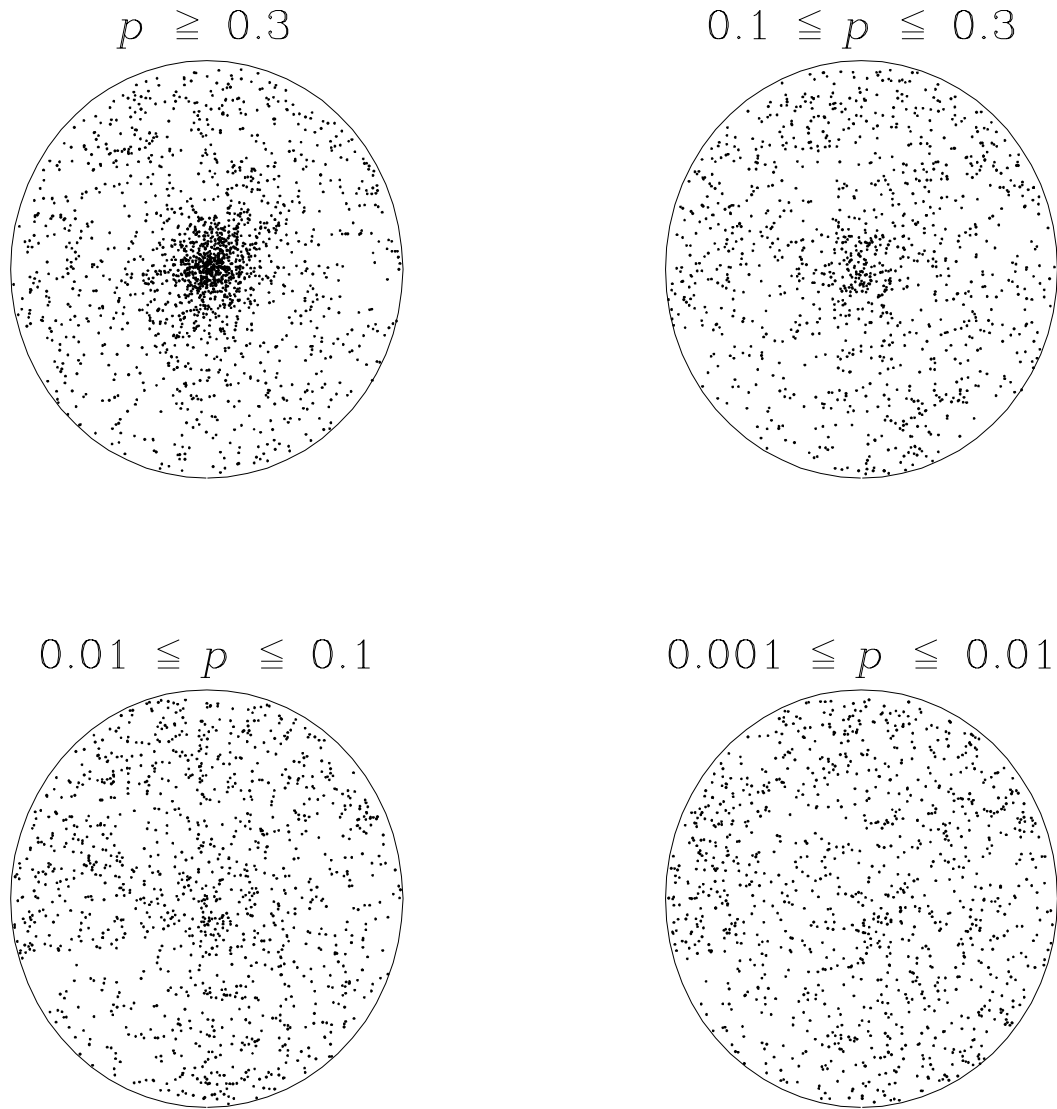


Fig. 5.— Spatial distribution of Pleiades candidates in the probability ranges $p > 0.3$; $0.1 \leq p < 0.3$; $0.01 \leq p < 0.1$; and $0.001 \leq p < 0.01$. The field apertures are each 10° in radius. Left corresponds to the eastern direction.

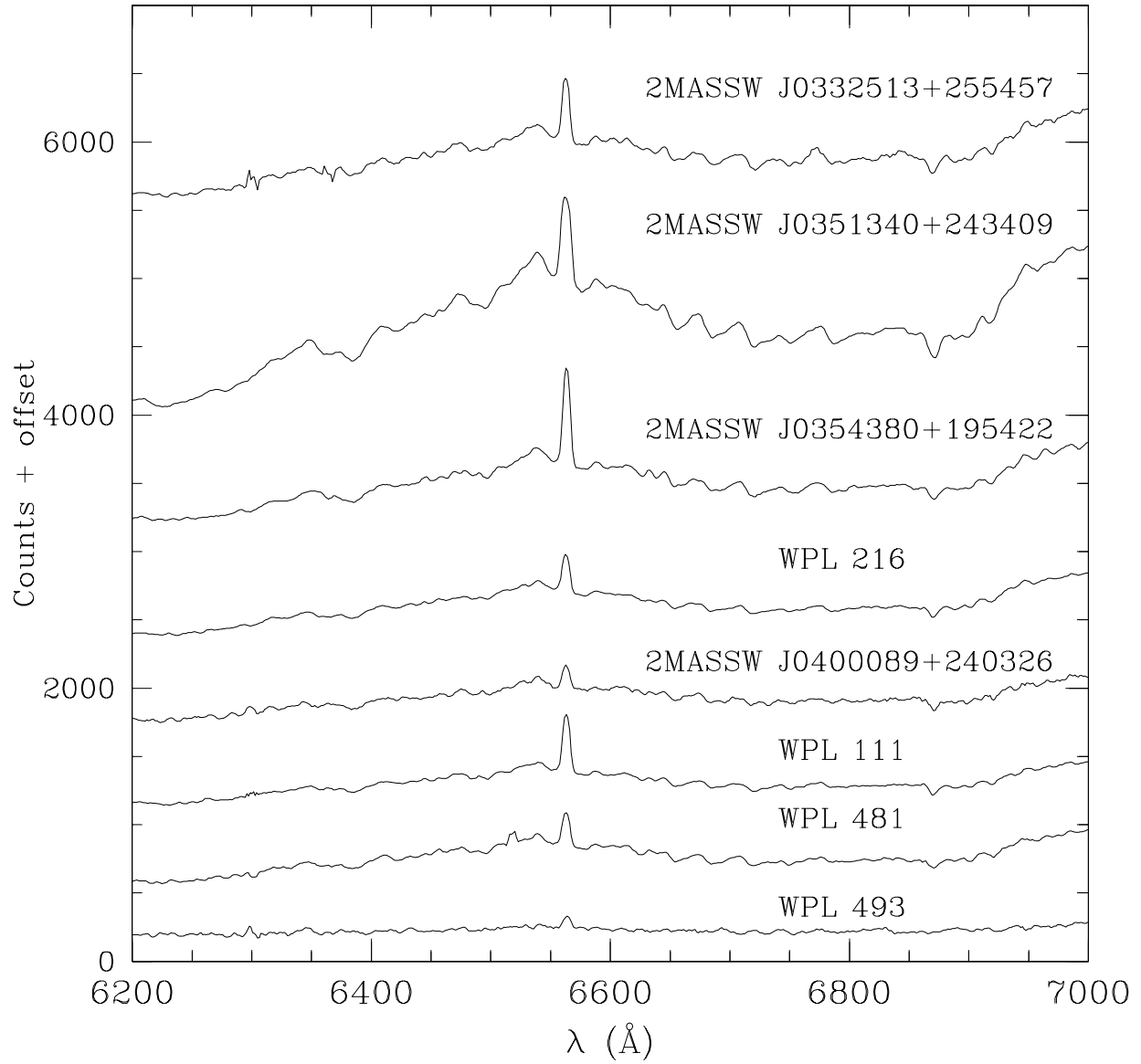


Fig. 6.— Smoothed spectra for representative Pleiades candidates that show H α emission. The WPL identifications are adopted from Adams (2000).

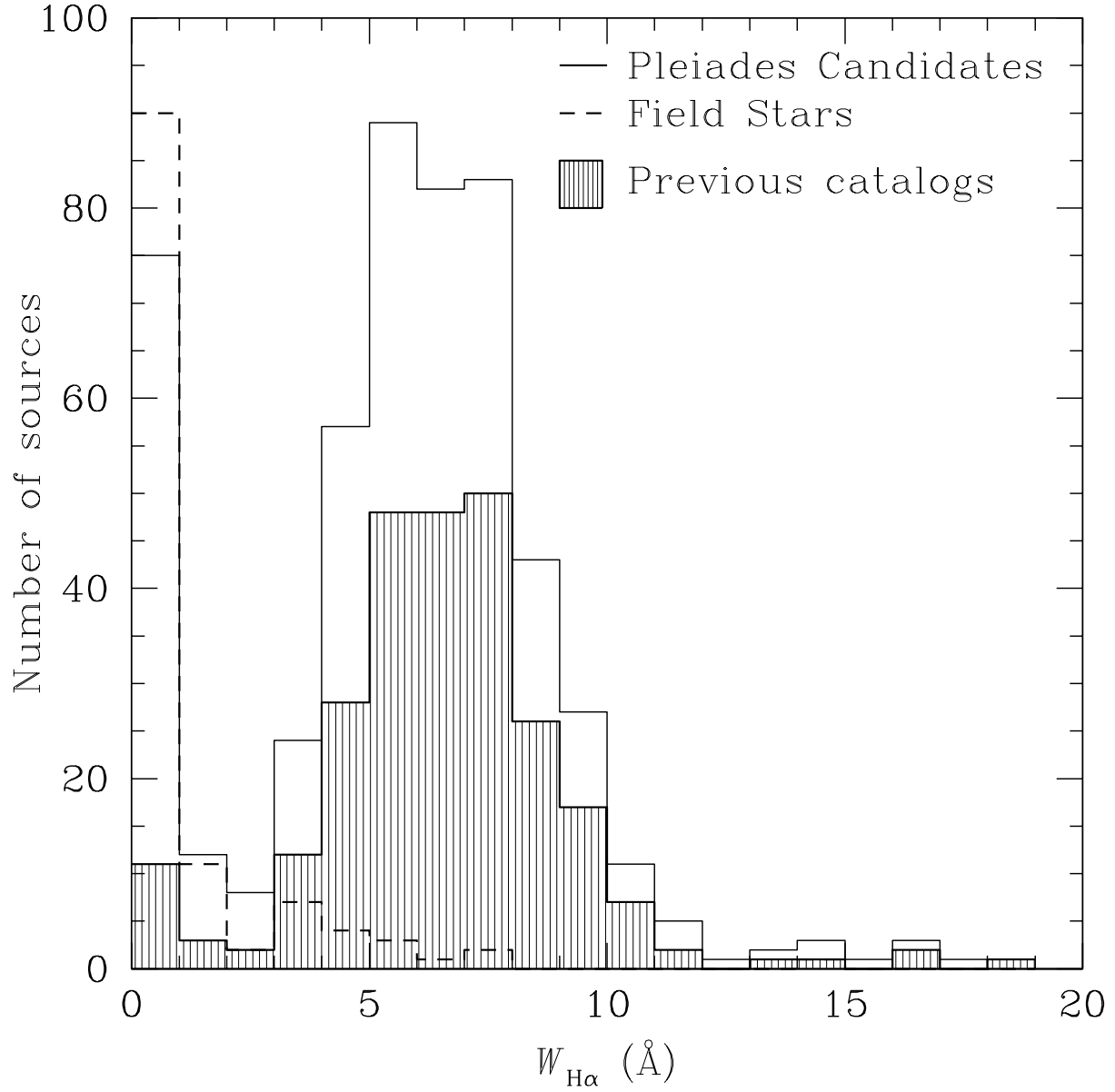


Fig. 7.— Histogram of H α equivalent widths $W_{H\alpha}$ for all sources in the Pleiades spectroscopic study. The shaded region indicates the fraction of candidates identified by previous Pleiades studies. The dashed line represents the distribution for the control sample.

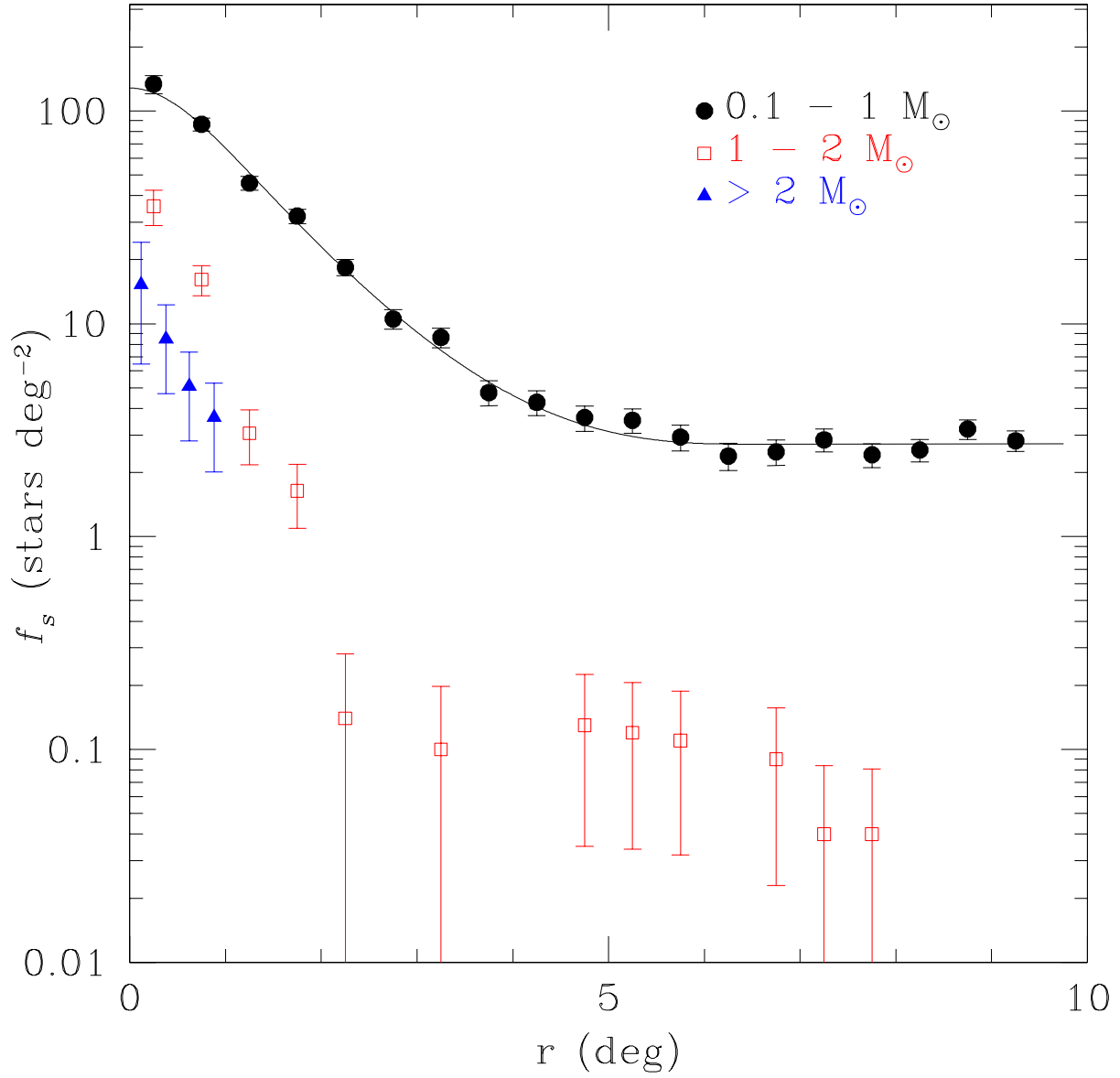


Fig. 8.— Radial profiles for surface density f_s , binned into annuli around the nominal center of the Pleiades, for three mass groups. The solid line shows the best fit single-mass King profile for the mass group $0.1 - 1 M_\odot$, superimposed on the mean background surface density. Error bars represent Poisson uncertainties in each bin.

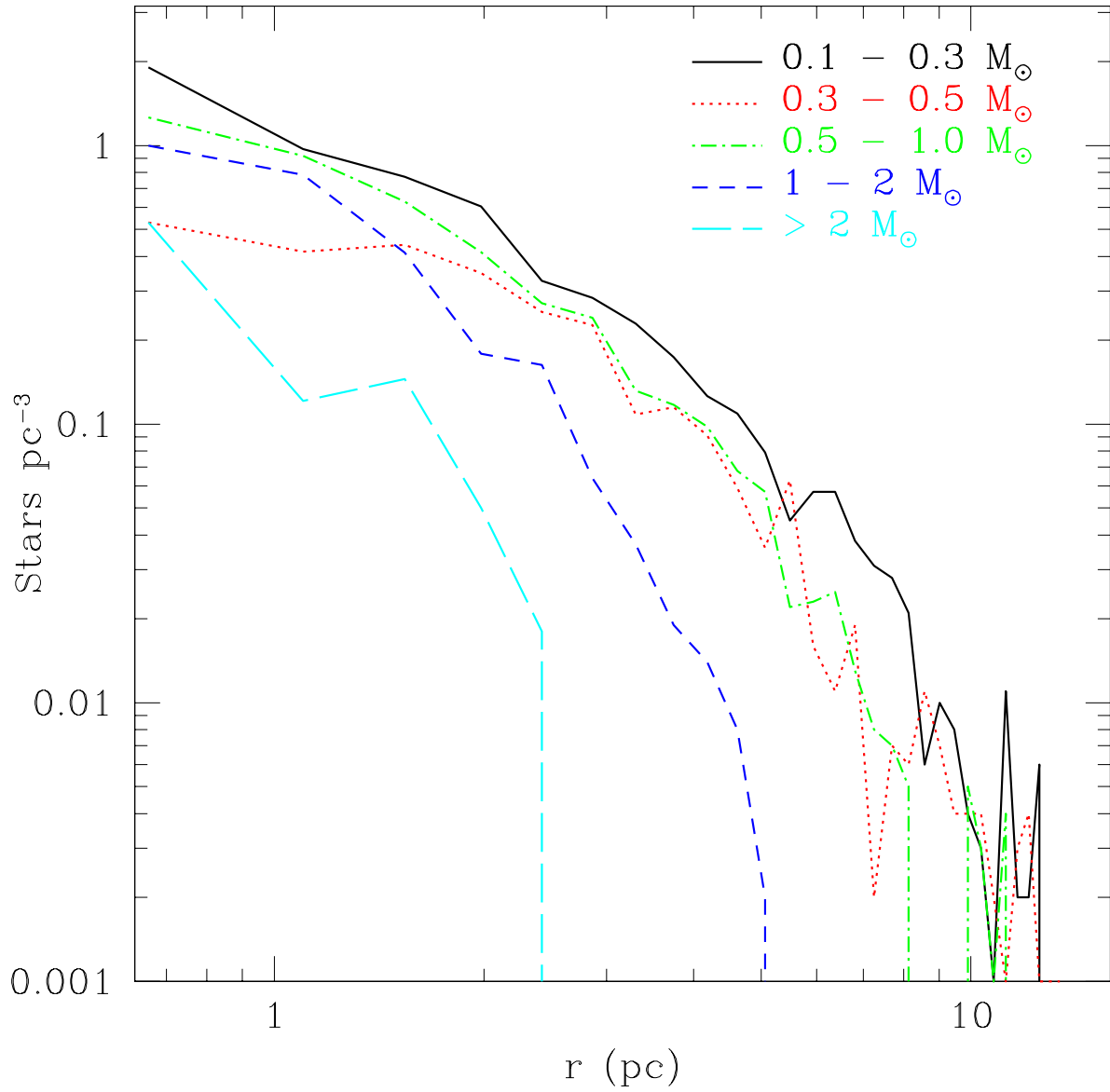


Fig. 9.— Approximate spatial density for Pleiades stars of different mass groups derived from a King model.

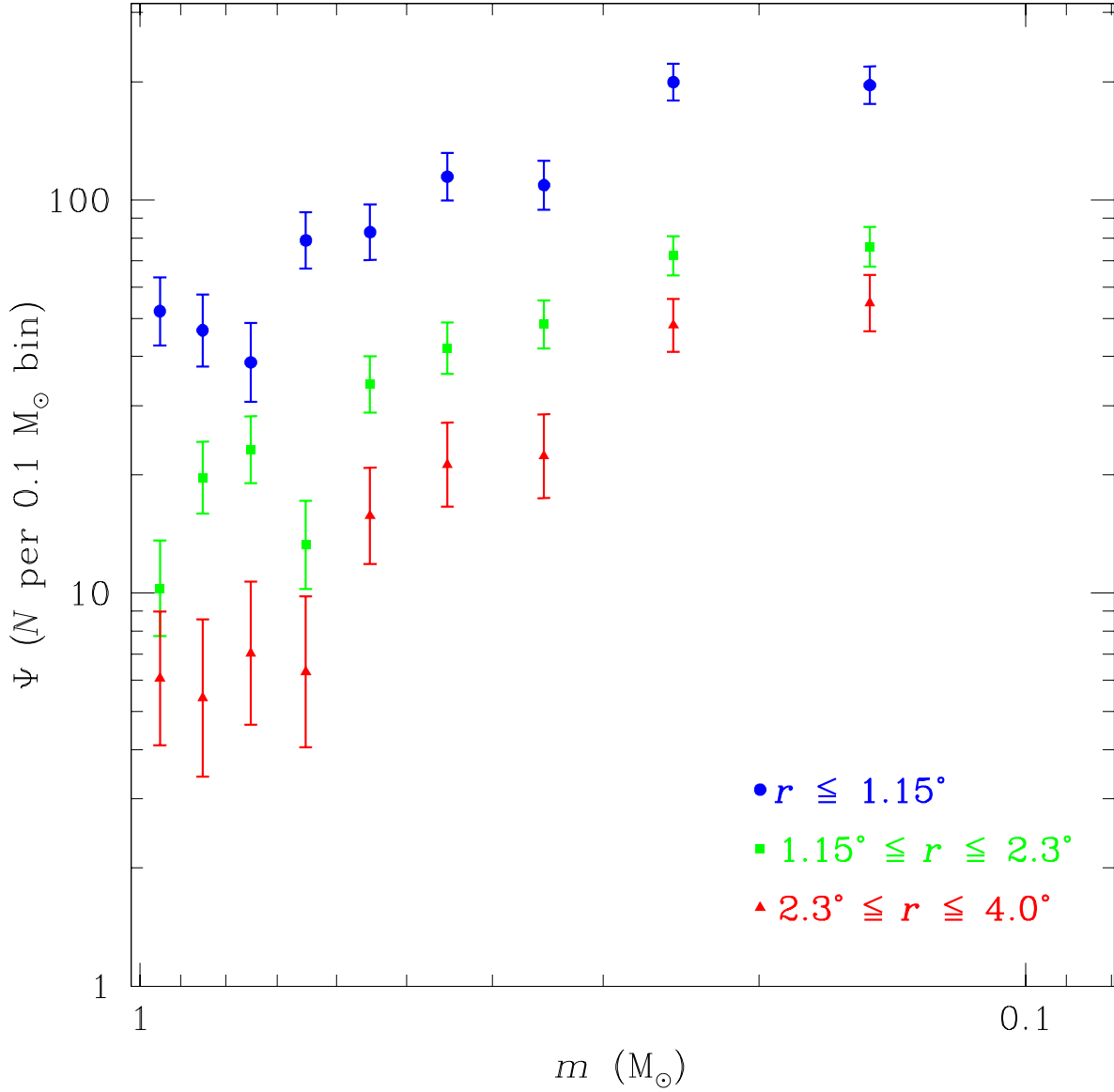


Fig. 10.— Radial dependence of the Pleiades mass function, corrected for field star contamination. The mass function for $r \leq 1.15^\circ$ has been shifted higher by a factor 2.5 for visual clarity. Error bars represent Poisson uncertainties. Note 1 core radius is roughly 1.15° .

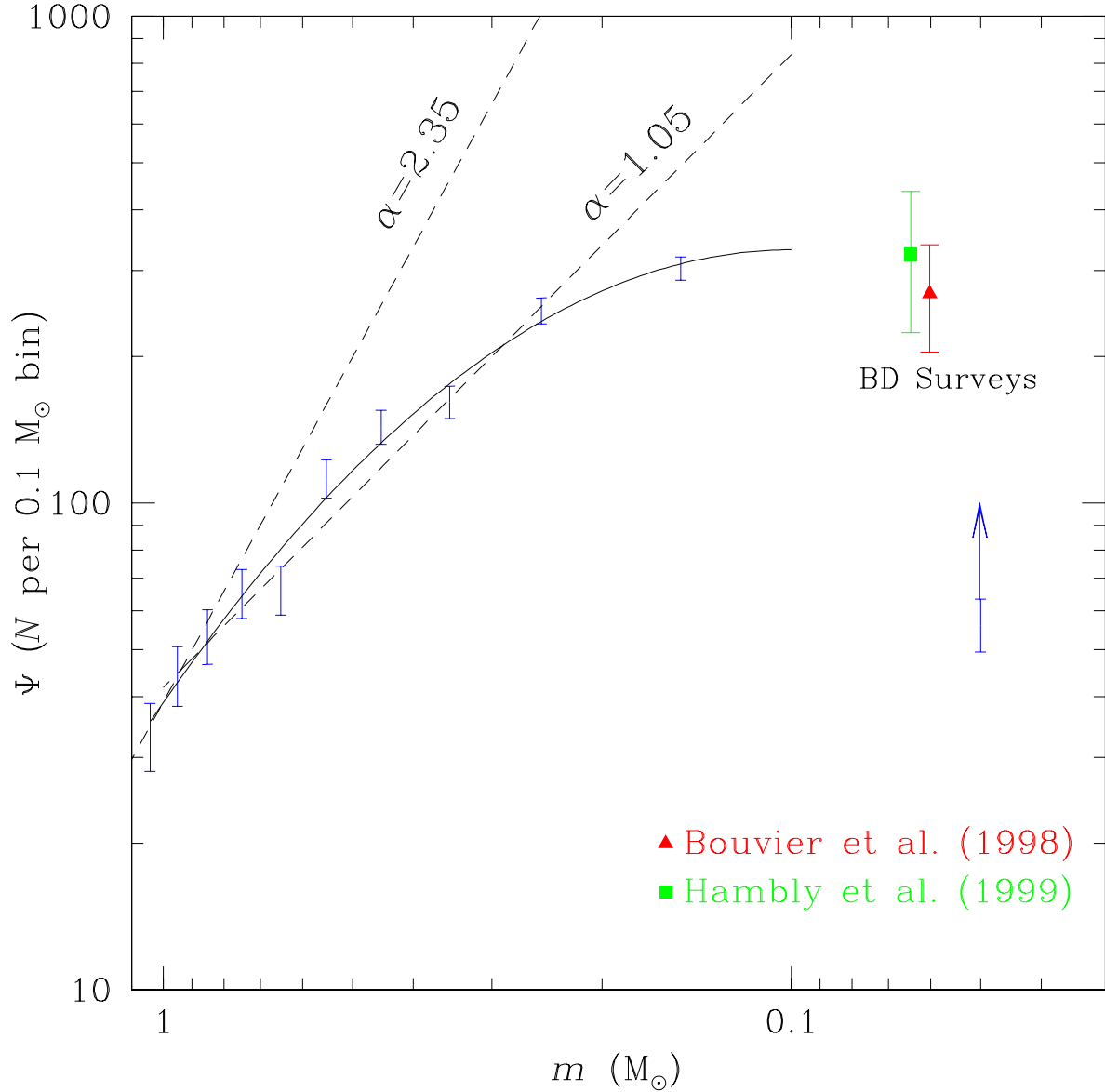


Fig. 11.— Pleiades mass function below $1 M_{\odot}$. The solid line indicates the best fit polynomial to $0.1 M_{\odot}$ where the sample becomes incomplete. Also shown are results from the brown dwarf surveys of Bouvier et al. (1998) (solid triangle) and Hambly et al. (1999) (solid box). For comparison, the dashed lines plot power law mass functions for the Salpeter case ($\alpha = 2.35$) and best fit ($\alpha = 1.05$) to the local field from $1 - 0.1 M_{\odot}$ (Reid & Gizis 1997), normalized to $\sim 1 M_{\odot}$.

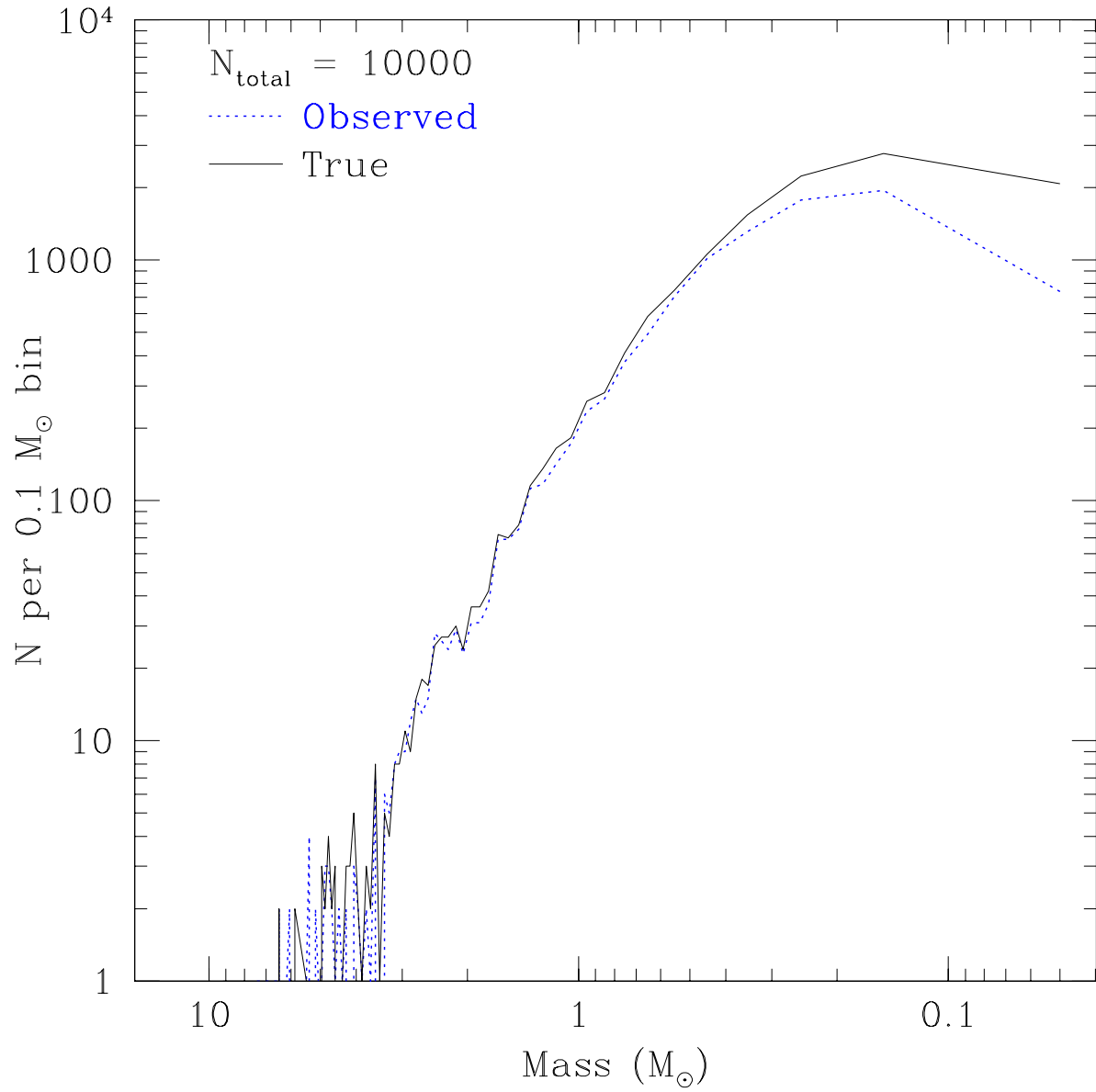


Fig. 12.— Simulated mass functions for a cluster of 10000 stars. In the observed case, all binary systems are unresolved.

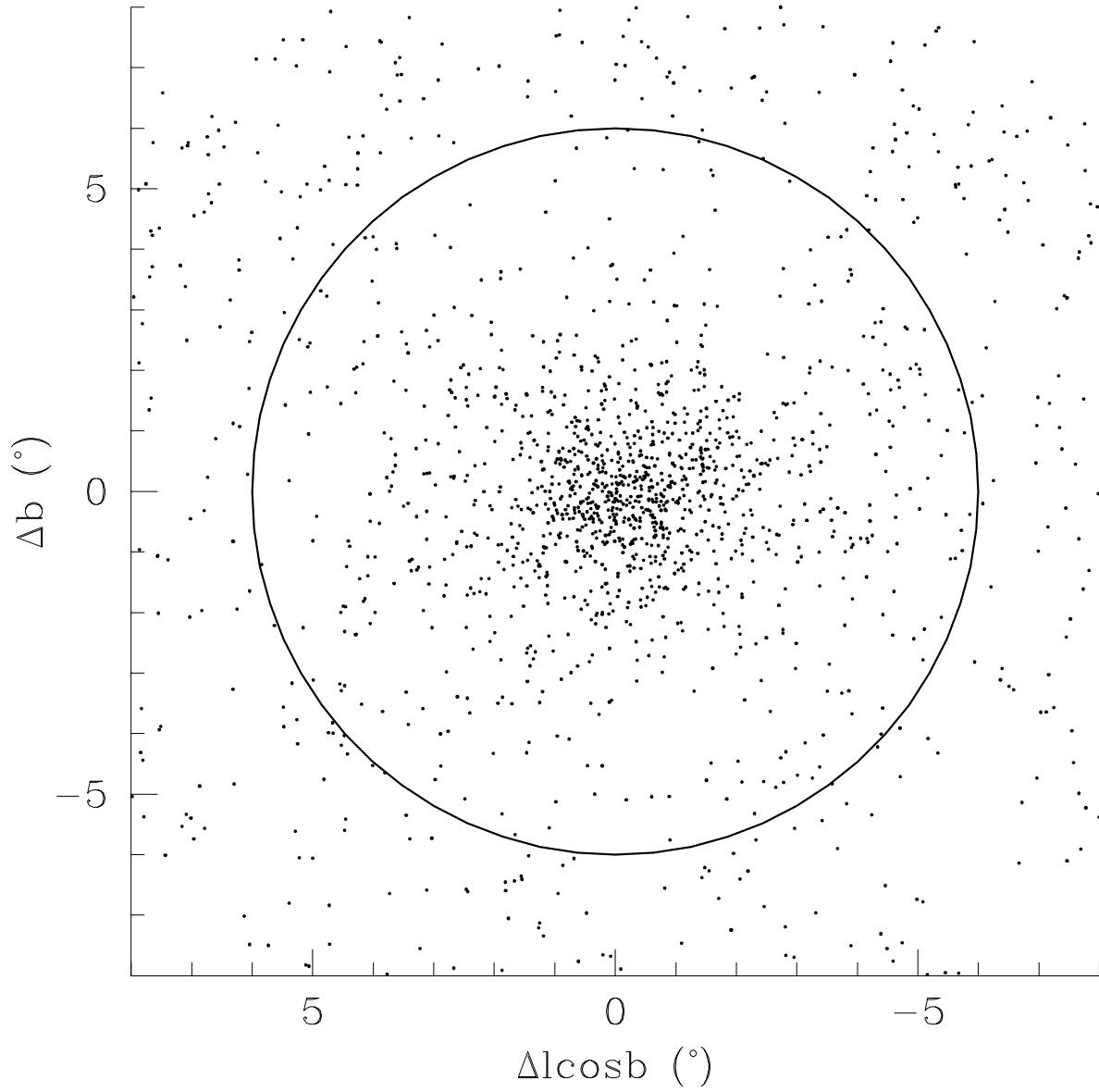


Fig. 13.— Spatial distribution in Galactic coordinates for $1 - 0.1 M_\odot$ Pleiades candidates. The circle traces the projection of the tidal radius derived from a total mass estimate of $\sim 800 M_\odot$. Nearly all objects outside the tidal radius in this plot belong to the field.

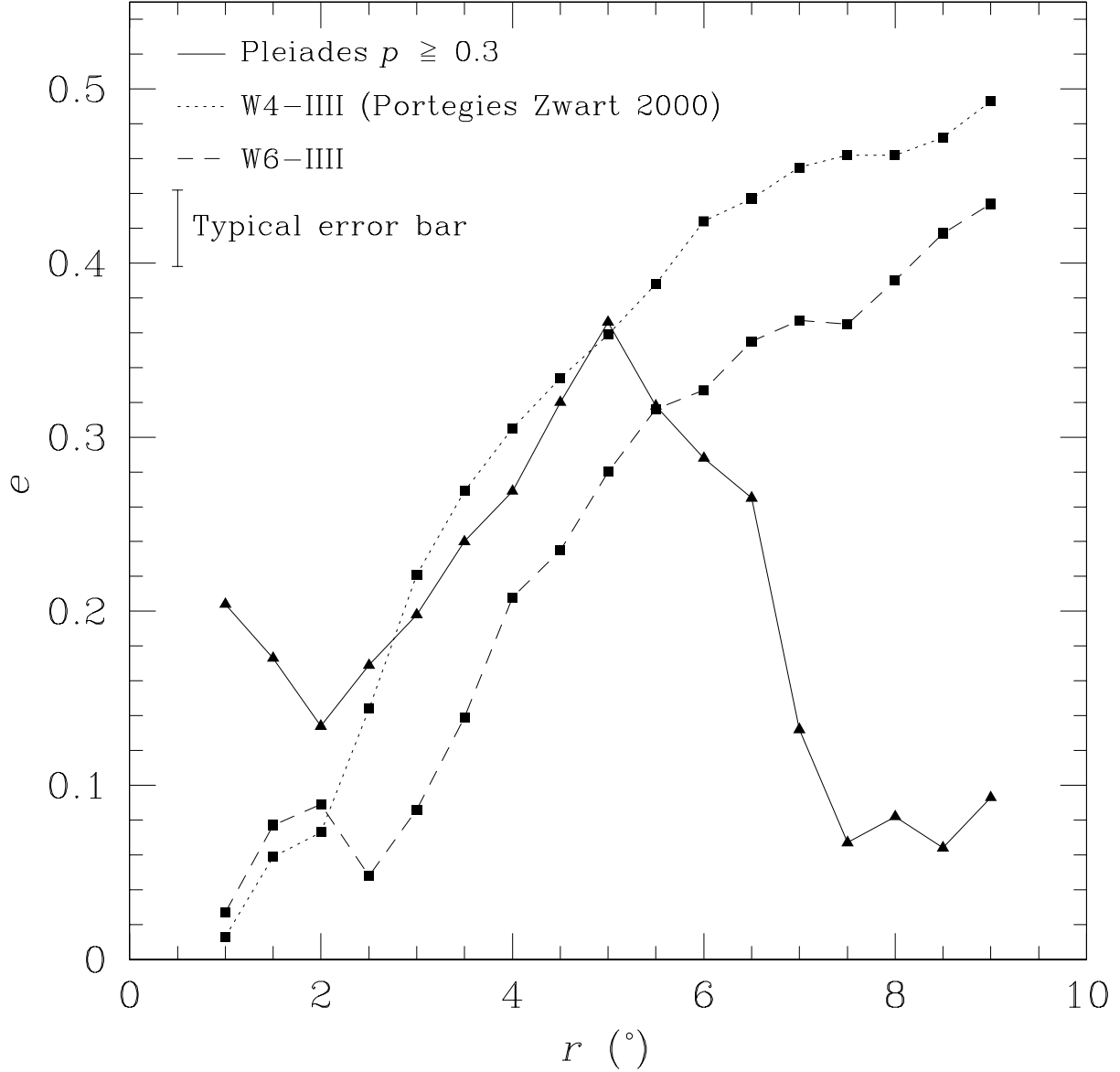


Fig. 14.— Ellipticity e of the Pleiades, plotted cumulatively *vs.* radial distance r , for stars with mass $1 - 0.1 M_{\odot}$ and $p \geq 0.3$. Dotted and broken and lines indicate analogous measurements for models W4-III and W6-III from Portegies Zwart (2000), simulated at 6 and 12 kpc from the Galactic center, at ages of 100 Myr. The simulated clusters have been scaled and projected onto the sky as if they were at the distance of the Pleiades. The error bars were estimated using Poisson uncertainties; only the typical error bar is shown for visual clarity.

Table 1. Coordinates for WIYN Hydra spectrograph fields with the number of Pleiades candidates, field control sources, and exposure time.

Date (2000 UT)	RA (J2000)	DEC	Candidates	Control	Exp. time (min.)
Nov 26 02:48	03 44 50	+24 32 47	43	0	90
Nov 26 05:23	03 44 54	+23 36 20	33	4	90
Nov 26 08:14	03 47 00	+24 06 00	49	3	90
Nov 26 10:34	03 49 01	+23 39 56	23	3	90
Nov 27 02:42	03 42 53	+24 03 53	48	4	90
Nov 27 04:47	03 47 07	+23 11 31	37	6	90
Nov 27 07:44	03 51 09	+24 09 15	20	1	90
Nov 27 09:49	03 48 50	+24 37 33	37	2	90
Nov 27 11:56	04 00 04	+23 49 00	17	6	30
Nov 28 02:38	03 50 49	+25 05 01	18	2	90
Nov 28 04:40	03 51 08	+23 11 37	13	6	90
Nov 28 07:13	03 43 06	+23 07 36	35	6	60
Nov 28 08:44	03 44 26	+25 29 21	31	6	60
Nov 28 10:54	03 58 24	+21 42 00	12	5	60
Nov 29 02:39	03 31 40	+26 12 00	10	5	45
Nov 29 03:56	03 34 48	+25 24 00	12	12	45
Nov 29 05:47	03 40 24	+25 27 33	31	9	45
Nov 29 07:00	03 49 24	+21 47 05	13	9	45
Nov 29 08:54	03 54 00	+19 42 00	7	9	30
Nov 29 09:54	03 38 47	+23 59 57	31	11	45
Nov 29 11:45	03 56 24	+26 42 00	8	4	45

Table 2. Number of Pleiades candidates distributed in $W_{H\alpha}$ (\AA) bins according to membership probability p , K_s magnitude, and radial distance r from the cluster center.

	0-1 \AA	1-3 \AA	3-5 \AA	5-7 \AA	7-9 \AA	9-11 \AA	> 11 \AA
p							
$0.001 \leq p \leq 0.01$	22	0	3	5	1	0	0
$0.01 \leq p \leq 0.1$	19	3	10	18	10	3	3
$0.1 \leq p \leq 0.3$	11	6	12	17	17	6	4
$0.3 \leq p \leq 1.0$	27	8	56	131	98	29	9
K_s							
$11 \leq K_s \leq 12$	3	2	14	27	15	1	0
$12 \leq K_s \leq 13$	33	2	17	85	69	23	7
$13 \leq K_s \leq 14$	29	8	46	55	38	14	7
$14 \leq K_s \leq 15$	14	5	4	4	4	0	2
r							
$0^\circ \leq r \leq 1^\circ$	14	5	33	84	62	20	8
$1^\circ \leq r \leq 2^\circ$	35	6	31	61	48	11	6
$2^\circ \leq r \leq 3^\circ$	11	2	11	14	12	5	0
$3^\circ \leq r \leq 4^\circ$	15	3	4	10	3	2	2
$4^\circ \leq r \leq 5^\circ$	3	1	2	2	1	0	0
$5^\circ \leq r \leq 6^\circ$	1	0	0	0	0	0	0